Geophys. J. Int. (2000) **141**, 605–622

Electromagnetic edge diffraction revisited: the transient field of magnetic dipole sources

Peter Weidelt

Institut für Geophysik und Meteorologie, Technische Universität Braunschweig, D-38106 *Braunschweig, Germany. E-mail: p.weidelt@tu-bs.de*

Accepted 1999 December 16. Received 1999 December 15; in original form 1999 August 9

SUMMARY

A surprisingly simple exact solution is derived for the transient electromagnetic field scattered by a perfectly conducting half-plane, which is embedded in a uniformly conducting host and energized by a unit step impulse of an arbitrarily oriented magnetic dipole. Despite its simplicity, the model has some relevance for geophysical applications (e.g. mineral exploration), provides insight into the physics of the transient scattering process, and has merits in validating numerical 2.5-D or 3-D codes.

The diffraction of electromagnetic waves at a perfectly conducting edge is one of the few vectorial diffraction problems that allows an exact treatment. In the past, attention has been confined to harmonic excitation in a lossless dielectric host, whereas the transient field in a lossy medium has escaped attention. In the quasi-static approximation in particular, this solution turns out to be simple compared to the explicit form of the field using harmonic excitation. However, even the inclusion of displacement currents, which may be necessary when applying transient electromagnetic methods to environmental geophysics, does not lead to complications.

The electric field and the time derivative of the magnetic field are given explicitly both in the quasi-static limit and with the inclusion of displacement currents. The late-time behaviour of the field is remarkable: whereas the full-space parts of these fields show the well-known $t^{-5/2}$ decay, the diffracted wave emerging from the edge decays only as t^{-2} and therefore dominates the field geometry at late times.

The appendices briefly treat the quasi-static transient field of a grounded electric dipole and sketch the formal solution for a perfectly conducting half-plane in a layered host.

Key words: diffraction, electromagnetic diffusion, electromagnetic induction, transient electromagnetic fields.

1 INTRODUCTION

In electromagnetic mineral exploration, a conducting half-plane is a simple interpretive model for a thin dyke of mineralization. A time-varying magnetic dipole, which approximately represents a transmitter coil, serves as an inducing source. Based on the work of Sommerfeld (1897), an exact solution for a perfectly conducting half-plane in an insulating host was given by Wesley (1958) and West (1960) (see also Grant & West 1965, pp. 520–528). Although this model already provides a good description of the geometrical shape of the induced magnetic field, the restriction to perfect conductors and insulators does not allow one to model adequately the observed frequency or transient response.

However, two simple complementary generalizations exist for the model of Wesley and West: (1) retaining the insulating host—the perfectly conducting half-plane is replaced by a half-plane of finite conductance (Weidelt 1983); and (2) retaining the perfectly conducting half-plane—the insulating host is replaced by a uniform full space of finite conductivity. The second generalization will be considered in this paper. The obvious shortcoming of the model is the assumption of a uniform full space, which does not allow one to take into account the air–earth interface. However, the appeal of the model is its analytical simplicity, which is lost when considering more complicated models. On using the Wiener–Hopf theory (Noble 1958) or its equivalents (Clemmow 1951), integral representations of the exact solutions can be obtained for a half-plane of finite conductance embedded in a uniformly conducting host or even for a *horizontal* half-plane of finite or infinite conductance in a layered host. For a perfectly conducting half-plane the solution is sketched in Appendix B.

Rigorous edge diffraction theory starts with Sommerfeld's exact solution for the diffraction of a plane wave in E- or

H-polarization at a perfectly conducting half-plane (Sommerfeld 1896). Subsequently, the field of a point source in the presence of a half-plane was given by Sommerfeld (1897) in its static limit and generalized by Macdonald (1915) to harmonic scalar wave propagation. Solutions of the vectorial diffraction problem at an edge have become possible only after the role of additional edge conditions was clarified by Meixner (1949), Copson (1950) and Jones (1950). Only these conditions, which ensure that the field singularity at the edge is not too strong so that the edge does not radiate any energy, grant the uniqueness of the solution. On this basis, Senior (1953) determined the diffraction of electromagnetic waves at a perfectly conducting half-plane, using an oscillating electric dipole as the source. Subsequently, alternative derivations of his results were given by Vandakurov (1954), Williams (1957) and Woods (1957). Chapter 11 of Born & Wolf (1983) is an excellent review of the basic facts of electromagnetic edge diffraction.

In the frequency domain, the solution given for an electric dipole in a dielectric host is easily adapted to a magnetic dipole in a host, in which both conduction currents and displacement currents are taken into account. Assuming that the source current is switched off at a time $t=0$, the decay of the induced transient electromagnetic field is obtained by a Fourier transform of the frequency response. The simple form of the resulting field components in the quasi-static regime is not seriously changed when displacement currents are included. These currents affect the very early time of the decay curve and have recently received attention in applying transient electromagnetic methods to shallow investigations in environmental geophysics (Pellerin *et al.* 1995, 1996).

Transient half-plane diffraction also plays a role in seismology, where it may give, for instance, a simplified model for the scattering of a pulsed plane wave at a crack (Pao & Mow 1973, Chapter 5; Fertig & Müller 1979).

At first glance it might be considered as a sheer anachronism that in an era of massive parallel computing approaches to sophisticated 3-D electromagnetic modelling problems, someone still dares to model perfectly conducting half-planes and uniform full spaces. However, the reasons for not refraining from it are three-fold.

(1) The problem is one of the few vectorial scattering problems for laterally non-uniform conductors that admits an exact solution.

(2) Although the model response in the frequency domain has essentially been known for 45 years, little or no attention has been paid to the transient response of a half-plane in a lossy host, which—unlike the explicit form of the frequency response—turns out to be quite simple, even if the displacement currents are retained.

(3) Despite its simplicity, the model might have some relevance in exploration geophysics and it can certainly be used for the validation of numerical 2.5- or 3-D codes.

The paper is organized as follows. Section 2 reviews the solution of the scattering problem in the frequency domain, which in turn is transformed to the quasi-static transient response in Section 3, and displacement currents are included in Section 4. The closing Section 5 discusses the approximate inclusion of an insulating air half-space. The two appendices briefly address the transient electric dipole and the construction of a formal solution for a horizontal perfectly conducting half-plane in a layered host.

2 THE TIME-HARMONIC RESPONSE

A point $\mathbf{r}$ is denoted both by Cartesian coordinates (x, y, z) and by cylindrical coordinates (r, φ, Ξ), $0 \le \varphi \le 2\pi$, related by

$$x = -\Xi, \quad y = r\cos\varphi, \quad z = -r\sin\varphi, \tag{2.1}$$

with z counted positive downwards (Fig. 1). The perfectly conducting half-plane is lying at $z=0$, $y \ge 0$ with the edge along the x-axis. The upper and lower sides of the half-plane correspond to $\varphi = 0$ and $\varphi = 2\pi$. The conductivity, permittivity and magnetic permeability of the surrounding uniform full space are, respectively, σ, ϵ and μ_0. In this section the scattering problem is treated in the frequency domain. In subsequent sections the field is transformed into the time domain.

An oscillating magnetic dipole with moment serves as a source, where $\tilde{\mathbf{m}}(\omega)$ at $\mathbf{r}_0 = (x_0, y_0, z_0) = (r_0, \varphi_0, -x_0)$, where ω is the angular frequency and a time factor $\exp(+i\omega t)$ is used throughout. The tilde denotes a physical quantity in the frequency domain. Including displacement currents, the governing equations in the uniform host outside the half-plane are

$$\nabla \times \tilde{\mathbf{H}} = (\sigma + i\omega\epsilon)\tilde{\mathbf{E}}, \tag{2.2}$$

$$\nabla \times \tilde{\mathbf{E}} = -i\omega\mu_0[\tilde{\mathbf{H}} + \tilde{\mathbf{m}}\delta(\mathbf{r}-\mathbf{r}_0)], \tag{2.3}$$

where $\tilde{\mathbf{H}}$ and $\tilde{\mathbf{E}}$ are the magnetic and electric field vectors and δ is the 3-D Dirac function. The elimination of $\tilde{\mathbf{E}}$ then leads to

$$\nabla \times \nabla \times \tilde{\mathbf{H}} + k^2\tilde{\mathbf{H}} = -k^2\tilde{\mathbf{m}}\delta(\mathbf{r}-\mathbf{r}_0), \tag{2.4}$$

or alternatively, with

$$\nabla \cdot \tilde{\mathbf{H}} = -\nabla \cdot [\tilde{\mathbf{m}}\delta(\mathbf{r}-\mathbf{r}_0)], \tag{2.5}$$

to

$$(\nabla^2 - k^2)\tilde{\mathbf{H}} = -\nabla\nabla \cdot [\tilde{\mathbf{m}}\delta(\mathbf{r}-\mathbf{r}_0)] + k^2\tilde{\mathbf{m}}\delta(\mathbf{r}-\mathbf{r}_0), \tag{2.6}$$

where

$$k^2 := i\omega\mu_0(\sigma + i\omega\epsilon), \quad \Re e\, k \ge 0. \tag{2.7}$$

To ensure a unique solution of the scattering problem, $\tilde{\mathbf{H}}$ has to satisfy the following conditions.

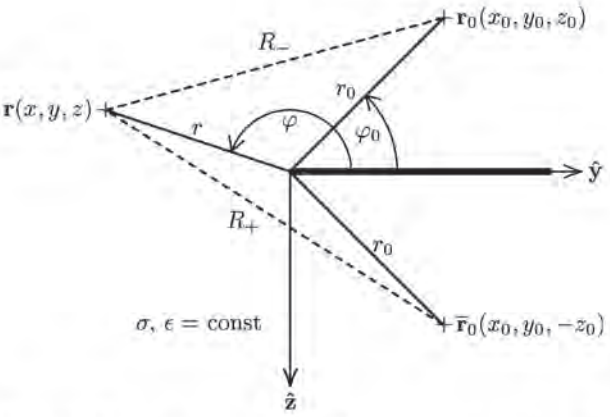

Figure 1. The perfectly conducting half-plane in a uniform host with conductivity σ and permittivity ϵ. The positions of the source dipole and its mirror image are denoted by $\mathbf{r}_0$ and $\bar{\mathbf{r}}_0$, respectively. The point of observation is $\mathbf{r}$. For ease of presentation it is assumed that $x = x_0$.

(1) *Boundary conditions:*

$$\tilde{H}_z = 0 \text{ at } \varphi = 0 \text{ and } \varphi = 2\pi . \tag{2.8}$$

(2) *Edge conditions* (e.g. Jones 1964, p. 569):

$$\tilde{H}_x = \mathcal{O}(1) \text{ and } \tilde{H}_y, \tilde{H}_z = \mathcal{O}(1/\sqrt{r}) \text{ for } r \to 0 . \tag{2.9}$$

The same edge conditions hold for the corresponding components of the electric field.

(3) *Radiation condition* (e.g. Jones 1964, p. 566): for $\sigma > 0$ it is required that uniformly in all directions

$$\tilde{\mathbf{H}} = \mathcal{O}\{\exp(-R \cdot \mathcal{R}e\, k)\} \text{ for } R \cdot \mathcal{R}e\, k \gg 1 , \tag{2.10}$$

where R is the distance from the origin.

(4) *Solenoidal condition:*

$$\nabla \cdot \tilde{\mathbf{H}} = 0 \text{ for } \mathbf{r} \neq \mathbf{r}_0 . \tag{2.11}$$

Let $k \neq 0$. Then the solenoidal condition is automatically satisfied if $\tilde{\mathbf{H}}$ satisfies (2.4) or enters as a supplementary condition if $\tilde{\mathbf{H}}$ satisfies (2.6). If $k = 0$, a field satisfying (2.4) requires (2.5) as a supplementary condition.

The corresponding scattering problem for an oscillating *electric* dipole in non-conducting surroundings is a classical problem (Senior 1953; Vandakurov 1954; Woods 1957; Williams 1957; Jones 1964, p. 593; Jones 1986, p. 566); the similar problem for an oscillating *magnetic* dipole in a conducting environment can be deduced from these results with only a few modifications.

Let $\tilde{\mathbf{m}} = \tilde{m}\,\hat{\mathbf{m}}$, where $\hat{\mathbf{m}}$ is a unit vector in the direction of the dipole moment. Essential ingredients to the solution are the two scalar potentials $\tilde{\Pi}_-$ and $\tilde{\Pi}_+$ satisfying

$$(\nabla^2 - k^2)\tilde{\Pi}_\pm = -\tilde{m}\,\delta(\mathbf{r} - \mathbf{r}_0) , \tag{2.12}$$

with the boundary conditions

$$\begin{aligned} &\tilde{\Pi}_-(\varphi = 0) = \tilde{\Pi}_-(\varphi = 2\pi) = 0 , \\ &\partial_z \tilde{\Pi}_+(\varphi = 0) = \partial_z \tilde{\Pi}_+(\varphi = 2\pi) = 0 . \end{aligned} \tag{2.13}$$

These potentials are given by

$$\tilde{\Pi}_\pm = \tilde{P}_- \pm \tilde{P}_+ \tag{2.14}$$

(e.g. Macdonald 1915; Senior 1953; Woods 1957; Jones 1964), where

$$\tilde{P}_\pm := \frac{\tilde{m}k}{4\pi^2} \int_{-\infty}^{u_\pm} K_1(kR_\pm \cosh u)\, du , \tag{2.15}$$

or alternatively

$$\tilde{P}_\pm = \frac{\tilde{m}\exp(-kR_\pm)}{8\pi R_\pm} + \frac{\tilde{m}k}{4\pi^2} \int_0^{u_\pm} K_1(kR_\pm \cosh u)\, du , \tag{2.16}$$

with

$$\sinh u_\pm := \frac{2\sqrt{rr_0}}{R_\pm} \cos\frac{\alpha_\pm}{2} , \tag{2.17}$$

$$\alpha_\pm := \varphi \pm \varphi_0 , \tag{2.18}$$

$$R_\pm^2 := \xi^2 + \eta^2 + \zeta_\pm^2 = \xi^2 + r^2 + r_0^2 - 2rr_0 \cos\alpha_\pm , \tag{2.19}$$

$$\xi := x - x_0 , \quad \eta := y - y_0 , \quad \zeta_\pm := z \pm z_0 . \tag{2.20}$$

$K_1(\cdot)$ is the modified Bessel function of the second kind and first order and R_- and R_+ are, respectively, the distances from the point of observation $\mathbf{r}$ to the source point $\mathbf{r}_0 = (x_0, y_0, z_0) = (r_0, \varphi_0, -x_0)$ and to its image point $\tilde{\mathbf{r}}_0 = (x_0, y_0, -z_0) = (r_0, 2\pi - \varphi_0, -x_0)$ (see Fig. 1). Examining the behaviour of $\tilde{P}_-$ for $\mathbf{r} \to \mathbf{r}_0$ and of $\tilde{P}_+$ for $\mathbf{r} \to \tilde{\mathbf{r}}_0$, it is found that

$$\tilde{P}_- \to \begin{cases} \dfrac{\tilde{m}}{4\pi R_-} , & \varphi \to \varphi_0 \\ 0 , & \varphi \to 2\pi + \varphi_0 \end{cases} \tag{2.21}$$

and

$$\tilde{P}_+ \to \begin{cases} 0 , & \varphi \to 2\pi - \varphi_0 \\ \dfrac{\tilde{m}}{4\pi R_+} , & \varphi \to 4\pi - \varphi_0 \end{cases} , \tag{2.22}$$

which is interpreted by Sommerfeld (1897) in terms of a space with two windings, where the *physical* winding $0 < \varphi < 2\pi$ contains the physical source and the *mathematical* winding $2\pi < \varphi < 4\pi$ the image source. In analogy to a branch cut in a two-fold Riemannian plane, these windings are connected along $\varphi = 2\pi$. At $\varphi = 4\pi$ the mathematical winding merges with the physical winding such that the potentials show a *continuous* variation with a period 4π but are discontinuous on the physical winding with a period 2π, i.e.

$$\tilde{P}_\pm(\varphi = 0) = \tilde{P}_\pm(\varphi = 4\pi) \neq \tilde{P}_\pm(\varphi = 2\pi) . \tag{2.23}$$

Physically, the discontinuity of $\tilde{P}_\pm$ describes the discontinuity of the horizontal magnetic field caused by the sheet currents and the discontinuity of the vertical electric field component caused by the surface charges.

Before considering the general case, we briefly digress to the special case $k \to 0$, corresponding to quasi-static conditions in a non-conducting surrounding, which has found widespread applications in geophysics (e.g. Wesley 1958; Grant & West 1965, p. 522; Hjelt 1968). In this case, (2.15) reduces to the solution of Sommerfeld (1897),

$$\begin{aligned} \tilde{P}_\pm &= \frac{\tilde{m}}{4\pi^2 R_\pm} \int_{-\infty}^{u_\pm} \frac{du}{\cosh u} \\ &= \frac{\tilde{m}}{8\pi R_\pm} \left[1 + \frac{2}{\pi} \tan^{-1}\left(\frac{2\sqrt{rr_0}}{R_\pm} \cos\frac{\alpha_\pm}{2} \right) \right] , \end{aligned} \tag{2.24}$$

and the resulting magnetic field is given by

$$\tilde{\mathbf{H}} = -\nabla\nabla_0 \cdot (\hat{\mathbf{m}}\tilde{\Pi}_+) , \tag{2.25}$$

with $\tilde{\Pi}_+$ obtained from (2.14) and (2.24). ∇_0 denotes differentiation with respect to source point coordinates.

Returning to the general case, we consider first the simple field of the oscillating magnetic dipole parallel to the edge, $\hat{\mathbf{m}} = \hat{\mathbf{x}}$. As an extension of (2.25), its magnetic field is given by

$$\tilde{\mathbf{H}} = -\nabla\nabla_0 \cdot (\hat{\mathbf{m}}\tilde{\Pi}_+) - k^2 \hat{\mathbf{m}}\tilde{\Pi}_+ , \tag{2.26}$$

with $\tilde{\Pi}_+$ now obtained from (2.14) and (2.15). By mere insertion it is seen that (2.26) solves the basic equation (2.6). Moreover, it satisfies the qualifying conditions (2.8)–(2.11). Hence the field can be derived from the one-component magnetic Hertz vector $\hat{\mathbf{x}}\tilde{\Pi}_+$.

When turning to the dipole in the y-direction, $\hat{\mathbf{m}} = \hat{\mathbf{y}}$, we find that (2.26) satisfies (2.6) and (2.8)–(2.10), but violates the solenoidal condition (2.11). A similar situation occurs for the dipole in the z-direction. Fortunately, this failure can be cured in both cases by adding to (2.26) extra terms that annihilate the non-zero divergence of the first terms. The resulting magnetic

field components for the three orthogonal dipoles are then

$\hat{\mathbf{m}} = \hat{\mathbf{x}}$:

$$\tilde{H}_{xx} = -(\partial_{xx_0} + k^2)\tilde{\Pi}_+ , \tag{2.27}$$

$$\tilde{H}_{yx} = -\partial_{yx_0}\tilde{\Pi}_+ , \tag{2.28}$$

$$\tilde{H}_{zx} = -\partial_{zx_0}\tilde{\Pi}_+ ; \tag{2.29}$$

$\hat{\mathbf{m}} = \hat{\mathbf{y}}$:

$$\tilde{H}_{xy} = -\partial_{xy_0}\tilde{\Pi}_+ , \tag{2.30}$$

$$\tilde{H}_{yy} = -(\partial_{yy_0} + k^2)\tilde{\Pi}_+ - c\,c_0\,\tilde{\Phi} , \tag{2.31}$$

$$\tilde{H}_{zy} = -\partial_{zy_0}\tilde{\Pi}_+ + s\,c_0\,\tilde{\Phi} ; \tag{2.32}$$

$\hat{\mathbf{m}} = \hat{\mathbf{z}}$:

$$\tilde{H}_{xz} = -\partial_{xz_0}\tilde{\Pi}_+ , \tag{2.33}$$

$$\tilde{H}_{yz} = -\partial_{yz_0}\tilde{\Pi}_+ + c\,s_0\,\tilde{\Phi} , \tag{2.34}$$

$$\tilde{H}_{zz} = -\partial_{zz_0}\tilde{\Pi}_+ - k^2\tilde{\Pi}_- - s\,s_0\,\tilde{\Phi} , \tag{2.35}$$

where

$$s := \sin(\varphi/2),\ c := \cos(\varphi/2),\ s_0 := \sin(\varphi_0/2),\ c_0 := \cos(\varphi_0/2) , \tag{2.36}$$

$$\tilde{\Phi} := \frac{\tilde{m}k^2}{2\pi^2\sqrt{rr_0}}\,K_0(k\bar{R}) \tag{2.37}$$

and

$$\bar{R}^2 := \xi^2 + (r + r_0)^2 . \tag{2.38}$$

Geometrically, $\bar{R}$ is the length of the shortest path, which connects the source point (or its mirror image) via a point at the edge with the point of observation. The edge is encountered at $\bar{x} = (x\,r_0 + x_0\,r)/(r_0 + r)$.

The additional $\tilde{\Phi}$ term has the desired property that the resulting magnetic field components are in harmony with the edge conditions (2.9). The angular function s ensures that $\tilde{H}_z$ vanishes at $\varphi = 0$ and $\varphi = 2\pi$, whereas the angular function c describes a discontinuity of the horizontal magnetic field components across the sheet caused by the sheet currents. Note that $\tilde{H}_{zz}$ requires the term $\tilde{\Pi}_-$ to satisfy the boundary condition (2.8).

As expected for magnetic point sources, the field components show the reciprocity

$$\tilde{H}_{k\ell}(\mathbf{r}|\,\mathbf{r}_0) = \tilde{H}_{\ell k}(\mathbf{r}_0|\,\mathbf{r}) , \quad k, \ell = x, y, z . \tag{2.39}$$

For the dipole in the y-direction we will now briefly justify the special form of $\tilde{\Phi}$ given in (2.37). Let $f = f(r, \varphi)$. Using

$$\begin{aligned} \partial_y f &= \cos\varphi\,\partial_r f - \frac{\sin\varphi}{r}\,\partial_\varphi f , \\ \partial_z f &= -\sin\varphi\,\partial_r f - \frac{\cos\varphi}{r}\,\partial_\varphi f \end{aligned} \tag{2.40}$$

and assuming that $\tilde{\Phi}$ does not depend on φ, the divergence formed from (2.30)–(2.32) is

$$\nabla\cdot\tilde{\mathbf{H}} = -k^2(\partial_y + \partial_{y_0})\tilde{\Pi}_+ - c\,c_0[1/(2r) + \partial_r]\tilde{\Phi} . \tag{2.41}$$

Taking into account the relations

$$\begin{aligned} &(\partial_y + \partial_{y_0})R_\pm = 0 , \quad (\partial_y + \partial_{y_0})u_\pm = \frac{r + r_0}{\bar{R}\sqrt{rr_0}}\cos(\alpha_\mp/2) , \\ &R_\pm\cosh u_\pm = \bar{R} , \quad \cos(\alpha_-/2) + \cos(\alpha_+/2) = 2c\,c_0 , \end{aligned} \tag{2.42}$$

we obtain

$$\begin{aligned} -k^2(\partial_y + \partial_{y_0})\tilde{\Pi}_+ &= -\frac{\tilde{m}k^3 c\,c_0(r + r_0)}{2\pi^2\bar{R}\sqrt{rr_0}}\,K_1(k\bar{R}) \\ &= \frac{\tilde{m}k^2 c\,c_0}{2\pi^2\sqrt{rr_0}}\,\partial_r K_0(k\bar{R}) . \end{aligned} \tag{2.43}$$

Therefore, with the solenoidal condition (2.11), (2.41) yields

$$\partial_r(\sqrt{r}\tilde{\Phi}) = \frac{\tilde{m}k^2}{2\pi^2\sqrt{r_0}}\,\partial_r K_0(k\bar{R}) , \tag{2.44}$$

from which (2.37) follows after integration. A non-vanishing constant of integration γ would add to $\tilde{\Phi}$ the term $\gamma/\sqrt{r}$, which violates the radiation condition (2.10). Consequently, $\gamma = 0$.

The solution (2.26) for the dipole in the x-direction can alternatively be written as

$$\tilde{\mathbf{H}} = \nabla\nabla\cdot(\hat{\mathbf{m}}\tilde{\Pi}_+) - k^2\hat{\mathbf{m}}\tilde{\Pi}_+ , \tag{2.45}$$

which also satisfies the solenoidal condition (2.11) for $\hat{\mathbf{m}} = \hat{\mathbf{y}}$, but violates for this choice, because $\tilde{\mathbf{H}} = \mathcal{O}(r^{-3/2})$ for $r \to 0$, the edge condition (2.9). Then additional terms have to be designed to remove this strong singularity. Of course, the final results agree with (2.30)–(2.32). However, the construction of the additional terms via the solenoidal condition is formally simpler than the conventional approach based on the edge condition.

3 THE QUASI-STATIC TRANSIENT RESPONSE

3.1 The quasi-static potentials in the time domain

Attention is confined to a sharp current shut-off, where the magnetic moment changes as

$$\mathbf{m}(t) = \begin{cases} \mathbf{m}_0, & t < 0 \\ \mathbf{0}, & t > 0 \end{cases} . \tag{3.1}$$

The response for an arbitrary source current function can then be obtained by Duhamel's theorem (e.g. Carlslaw & Jaeger 1963). Using the Fourier transform pair

$$f(t) = \frac{1}{2\pi}\int_{-\infty}^{+\infty}\tilde{f}(\omega)\,e^{i\omega t}\,d\omega , \quad \tilde{f}(\omega) = \int_{-\infty}^{+\infty} f(t)\,e^{-i\omega t}\,dt , \tag{3.2}$$

we obtain

$$\tilde{\mathbf{m}} = \lim_{\delta\to 0^+}\frac{\mathbf{m}_0}{\delta - i\omega} , \tag{3.3}$$

where δ is a small positive quantity, which keeps the pole of $\tilde{\mathbf{m}}$ in the lower frequency plane. Since in applications the magnetic signal is mostly recorded by induction-coil magnetometers, which measure the time derivative $\dot{\mathbf{H}}$, we shall confine our attention to this—simpler—quantity rather than to $\mathbf{H}$.

Therefore, we consider

$$\dot{\Pi}_\pm = \dot{P}_- \pm \dot{P}_+ \quad \text{with} \quad \dot{P}_\pm = \frac{1}{2\pi}\int_{-\infty}^{+\infty} i\omega \tilde{P}_\pm \, e^{i\omega t}\, d\omega , \tag{3.4}$$

where $\tilde{P}_\pm$ is given in (2.15).

The diffusive quasi-static response neglecting the displacement currents is applicable if the time elapsed after the current shut-off is much greater than the traveltime from the source to the point of observation (of the order of 10^{-6} s in geophysical applications) and much greater than the decay time of free charges in the conductor (typically $< 10^{-7}$ s; see Section 4). For instrumental reasons, the first time channel in transient electromagnetic prospecting rarely falls much below 10^{-5} s. Therefore, it is the quasi-static response, i.e. $k^2 = i\omega\mu_0\sigma$, that at present has the most interesting applications in geophysics.

Using the relation $K_1(\cdot) = -K_0'(\cdot)$ and the result

$$\frac{1}{2\pi}\int_{-\infty}^{+\infty} K_0(kR)\, e^{i\omega t}\, d\omega = \frac{1}{2t}\exp\left(-\frac{\mu_0\sigma R^2}{4t}\right), \tag{3.5}$$

we obtain with $\mathbf{m}_0 = m_0\hat{\mathbf{m}}$ after changing the order of integration

$$\dot{P}_\pm = -\frac{m_0 \cdot \exp[-R_\pm^2/(4\tau)]}{8\mu_0\sigma\sqrt{\pi^3\tau^3}} \cdot w_\pm \tag{3.6}$$

with the normalized time (dimension of a squared length)

$$\tau := \frac{t}{\mu_0\sigma} \tag{3.7}$$

and

$$w_\pm := \frac{1}{\sqrt{\pi}}\int_{-\infty}^{\beta_\pm} e^{-u^2}\, du = \frac{1}{2}\,[1 + \operatorname{erf}(\beta_\pm)], \tag{3.8}$$

where

$$\beta_\pm := \sqrt{\frac{rr_0}{\tau}}\cos\frac{\alpha_\pm}{2} \quad \text{and} \quad \operatorname{erf}(x) := \frac{2}{\sqrt{\pi}}\int_0^x e^{-u^2}\, du . \tag{3.9}$$

For a dipole at point $\mathbf{r}_0$ of a uniform full space we have in the frequency domain

$$\tilde{\mathbf{H}} = \nabla\nabla\cdot(\hat{\mathbf{m}}\tilde{\Pi}_0) - k^2\hat{\mathbf{m}}\tilde{\Pi}_0 \quad \text{with} \quad \tilde{\Pi}_0 = \frac{\tilde{m}\cdot\exp(-kR_-)}{4\pi R_-}, \tag{3.10}$$

and therefore

$$\dot{\Pi}_0 = \frac{1}{2\pi}\int_{-\infty}^{+\infty} i\omega\tilde{\Pi}_0\, e^{i\omega t}\, d\omega = -\frac{m_0\cdot\exp[-R_-^2/(4\tau)]}{8\mu_0\sigma\sqrt{\pi^3\tau^3}} . \tag{3.11}$$

Hence, the cofactor of $w_\pm$ in (3.6) can be interpreted as a quasi-static full-space response, where R_- refers to the physical source and R_+ to its mirror image. The functions $w_\pm$ with $0 \le w_\pm \le 1$ are space- and time-dependent weights, which control the contribution of each source and thus describe the intensity variations when moving between light and shadow (see the detailed discussion below).

The transient form of the additional $\tilde{\Phi}$ term (2.37) is

$$\Phi = \frac{1}{2\pi}\int_{-\infty}^{+\infty}\tilde{\Phi}\, e^{i\omega t}\, d\omega = -\frac{m_0\cdot\exp[-\overline{R}^2/(4\tau)]}{4\pi^2\tau\sqrt{rr_0}} , \tag{3.12}$$

$$\dot{\Phi} = \frac{1}{2\pi}\int_{-\infty}^{+\infty} i\omega\tilde{\Phi}\, e^{i\omega t}\, d\omega = \frac{m_0\cdot\exp[-\overline{R}^2/(4\tau)]}{4\pi^2\mu_0\sigma\tau^2\sqrt{rr_0}}\left(1-\frac{\overline{R}^2}{4\tau}\right). \tag{3.13}$$

3.2 The transient quasi-static magnetic field

With (3.13) and $\dot{\Pi}_\pm = \dot{P}_- \pm \dot{P}_+$, the transient versions of (2.27)–(2.35) are

$\hat{\mathbf{m}} = \hat{\mathbf{x}}$:

$$\dot{H}_{xx} = -(\partial_{xs_0} + \partial_\tau)\dot{\Pi}_+ , \tag{3.14}$$

$$\dot{H}_{yx} = -\partial_{yx_0}\dot{\Pi}_+ , \tag{3.15}$$

$$\dot{H}_{zx} = -\partial_{zx_0}\dot{\Pi}_+ ; \tag{3.16}$$

$\hat{\mathbf{m}} = \hat{\mathbf{y}}$:

$$\dot{H}_{xy} = -\partial_{xy_0}\dot{\Pi}_+ , \tag{3.17}$$

$$\dot{H}_{yy} = -(\partial_{yy_0} + \partial_\tau)\dot{\Pi}_+ - c\,c_0\,\dot{\Phi} , \tag{3.18}$$

$$\dot{H}_{zy} = -\partial_{zy_0}\dot{\Pi}_+ + s\,c_0\,\dot{\Phi} ; \tag{3.19}$$

$\hat{\mathbf{m}} = \hat{\mathbf{z}}$:

$$\dot{H}_{xz} = -\partial_{xz_0}\dot{\Pi}_+ , \tag{3.20}$$

$$\dot{H}_{yz} = -\partial_{yz_0}\dot{\Pi}_+ + c\,s_0\,\dot{\Phi} , \tag{3.21}$$

$$\dot{H}_{zz} = -\partial_{zz_0}\dot{\Pi}_+ - \partial_\tau\dot{\Pi}_- - s\,s_0\,\dot{\Phi} . \tag{3.22}$$

The subsequent differentiations are simplified on using the identities

$$\partial_y\beta_\pm = +\sqrt{\frac{r_0}{4\tau r}}\cos\frac{\alpha_\mp}{2} , \quad \partial_z\beta_\pm = -\sqrt{\frac{r_0}{4\tau r}}\sin\frac{\alpha_\mp}{2} \tag{3.23}$$

and

$$R_\pm^2 + 4\tau\beta_\pm^2 = \overline{R}^2 . \tag{3.24}$$

By the latter identity, $\dot{\Phi}$ terms and differentiated $\dot{\Pi}_\pm$ terms merge because of identical exponents. The time derivative of the transient magnetic field is then

$$\dot{\mathbf{H}}(\mathbf{r}|\,\mathbf{r}_0;\,t) = \dot{\mathscr{H}}(\mathbf{r}|\,\mathbf{r}_0;\,t)\,\hat{\mathbf{m}} \tag{3.25}$$

with

$$\dot{\mathscr{H}} = w_-\dot{\mathscr{H}}_- + w_+\dot{\mathscr{H}}_+ + \dot{\mathscr{D}} , \tag{3.26}$$

where the diffraction tensors $\dot{\mathscr{H}}_\pm$ and $\dot{\mathscr{D}}$ are given in Cartesian coordinates (x, y, z) by

$$\dot{\mathscr{H}}_\pm = p_\pm\cdot\begin{pmatrix} \xi^2+\Delta_\pm & \xi\eta & \mp\xi\zeta_\pm \\ \xi\eta & \eta^2+\Delta_\pm & \mp\eta\zeta_\pm \\ \xi\zeta_\pm & \eta\zeta_\pm & \mp(\zeta_\pm^2+\Delta_\pm) \end{pmatrix}, \tag{3.27}$$

$$\dot{\mathscr{D}} = \overline{p}\cdot\begin{pmatrix} 2rr_0\,c\,c_0 & \xi r\,c\,c_0 & -\xi r\,c\,s_0 \\ -\xi r_0\,c\,c_0 & (\Delta+2rr_0)\,c\,c_0 & -(\Delta+r_0^2+rr_0)\,c\,s_0 \\ \xi r_0\,s\,c_0 & -(\Delta+r^2+rr_0)\,s\,c_0 & [\Delta+(r+r_0)^2]\,s\,s_0 \end{pmatrix} \tag{3.28}$$

with

$$\Delta_\pm := 4\tau - R_\pm^2\,, \quad \Delta := 3\tau + r^2\cos\varphi + r_0^2\cos\varphi_0 - \overline{R}^2\,, \tag{3.29}$$

$$p_\pm := -\frac{m_0\cdot\exp[-R_\pm^2/(4\tau)]}{32\mu_0\sigma\sqrt{\pi^3\tau^7}}\,, \quad \overline{p} := -\frac{m_0\cdot\exp[-\overline{R}^2/(4\tau)]}{16\mu_0\sigma\pi^2\tau^3\sqrt{r\,r_0}}\,. \tag{3.30}$$

The first column of the diffraction tensors gives the Cartesian magnetic field components for a source dipole in the x-direction. Similarly, the second and third columns refer to dipoles in the y- and z-directions, respectively. Reciprocity is guaranteed by the symmetry

$$\dot{\mathscr{H}}(\mathbf{r}|\mathbf{r}_0;\,t) = \dot{\mathscr{H}}^{\mathrm{T}}(\mathbf{r}_0|\mathbf{r};\,t)\,, \tag{3.31}$$

where $^{\mathrm{T}}$ denotes transposition. The alternative product representation

$$\dot{\mathscr{D}} = \overline{p}\cdot\mathrm{diag}(c,\,c,\,s)\begin{pmatrix} 2rr_0 & \xi r & -\xi r \\ -\xi r_0 & \Delta+2rr_0 & -(\Delta+r_0^2+rr_0) \\ \xi r_0 & -(\Delta+r^2+rr_0) & \Delta+(r+r_0)^2 \end{pmatrix} \times \mathrm{diag}(c_0,\,c_0,\,s_0) \tag{3.32}$$

further clarifies the structure of $\dot{\mathscr{D}}$.

Eq. (3.26) represents $\dot{\mathbf{H}}$ in terms of three sources: $\dot{\mathscr{H}}_-$ describes the incident field, $\dot{\mathscr{H}}_+$ results from the image source and describes the field reflected at a perfectly conducting *full* plane, and $\dot{\mathscr{D}}$ is the diffracted field emanating from the edge. The relative size of the weights $w_\pm$, $0\le w_+\le 1$, which describe the contributions from the first two sources, can be understood with reference to the geometrical optics field (Fig. 2). In the diffusive regime considered here, the discontinuities occurring in geometrical optics between light and shadow are replaced by continuous transitions. Without restriction of generality, attention is confined to a source in $z\le 0$, i.e. $0\le\varphi_0\le\pi$. In geometrical optics the incident field is present in region A, corresponding to $0\le\varphi<\varphi_0+\pi$ or $\cos(\alpha_-/2)>0$. According to (3.8), in the diffusive regime a weight $w_->1/2$ is assigned to points that in geometrical optics lie in the illuminated region. On the other hand, the incident field is absent in the shadow region C with $\varphi_0+\pi<\varphi\le 2\pi$ corresponding to $\cos(\alpha_-/2)<0$ or $w_-<1/2$. Significant contributions from the image source will occur at points that are reached by a ray reflected at the half-plane (that is, with a point of reflection in $y>0$). These points, for which the image source is *invisible*, lie in region B with $0\le\varphi<\pi-\varphi_0$, corresponding to $\cos(\alpha_+/2)>0$ or $w_+>1/2$. On the other hand, the image source has small weights at points where it is visible, that is, for $\pi-\varphi_0<\varphi\le 2\pi$ with $\cos(\alpha_+/2)<0$ or $w_+<1/2$ (region D). For early time, $\tau/(rr_0)\ll 1$, the weights tend to unity in the illuminated regions A and B and to zero in the shadow regions C and D. For late time, $\tau/(rr_0)\gg 1$, all weights approach $1/2$.

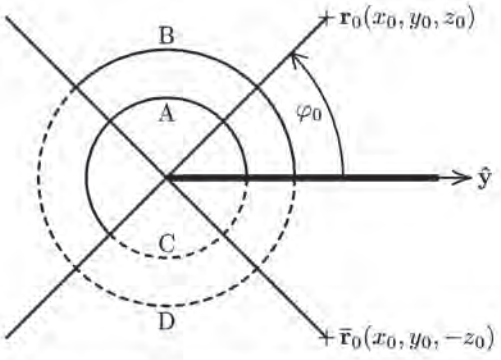

Figure 2. The sectors of illumination and shadow for the source dipole are sector A (full line) with $w_->0.5$ and sector C (dashed line) with $w_-<0.5$. The image source contributes to the scattered field mostly in the sector where it is invisible, i.e. $w_+>0.5$ in sector B (full line) and $w_+<0.5$ in sector D (dashed line).

The term $\dot{\mathscr{D}}$ shows in its radial and angular dependence the expected characteristic signature of an edge diffraction. Since $\overline{q}=\mathcal{O}(1/\sqrt{r})$ for $r\to 0$, the components $\dot{H}_y$ and $\dot{H}_z$ along with H_y and H_z are not more singular than allowed by the edge condition (2.9). Moreover, the magnetic field component along the edge resulting from $\dot{\mathscr{D}}$ is $\mathcal{O}(\sqrt{r})$, such that—including the contributions from $\dot{\mathscr{H}}_-$ and $\dot{\mathscr{H}}_+$—we have $H_x=\mathcal{O}(1)$, in full accord with (2.9). Recalling that $\overline{R}$ is the length of the shortest path connecting the source via the edge with the observer, the dominant dependence of $\dot{\mathscr{D}}$ on $\overline{R}$ is again in agreement with the physical interpretation of $\dot{\mathscr{D}}$.

Due to the discontinuity of the weights across the half-plane, the first two terms of (3.26) give rise to discontinuous horizontal magnetic field components, which take account of the sheet currents. Since $w_-=w_+$ for $\varphi=0$ and $\varphi=2\pi$, the resulting vertical component vanishes at both sides.

The horizontal magnetic components resulting from $\dot{\mathscr{D}}$ involve the factor $c=\cos(\varphi/2)$, which changes its sign when crossing the half-plane from $\varphi=0$ to $\varphi=2\pi$ and thus accounts for the discontinuous magnetic field due to the sheet currents. On the other hand, the horizontal magnetic field of these currents vanishes for $\varphi=\pi$, as expected for geometrical reasons. The angular dependence of the vertical magnetic field component of the edge diffraction field is controlled by the factor $s=\sin(\varphi/2)$, such that this component vanishes for $\varphi=0$ and $\varphi=2\pi$, whereas for $\varphi=\pi$ the sheet currents contribute only to this component.

Of interest is the late-time dependence of $\dot{\mathbf{H}}$. The elements of $\dot{\mathscr{H}}_\pm$ with the slowest decay are the diagonal elements, which show the $t^{-5/2}$ dependence familiar for a uniform half- or full space. The edge diffraction y- and z-components of a dipole in the y- or z-direction exhibit an even slower t^{-2} decay. Characterizing the late-time transient field of a dipole source by the component with the slowest decay, the x-dipole decays as $t^{-5/2}$ and the y- or z-dipole as t^{-2}.

3.3 The transient quasi-static electric field

Addressing now the electric field $\mathbf{E}=(1/\sigma)\nabla\times\mathbf{H}$, we obtain from (3.14)–(3.22)

$\hat{\mathbf{m}}=\hat{\mathbf{x}}$:

$$E_{xx}=0\,, \tag{3.33}$$

$$E_{yx}=-\mu_0\partial_z\dot{\Pi}_+\,, \tag{3.34}$$

$$E_{zx}=+\mu_0\partial_y\dot{\Pi}_+\,, \tag{3.35}$$

$\hat{\mathbf{m}} = \hat{\mathbf{y}}$:

$$E_{xy} = -\mu_0 \partial_{z_0} \dot{\Pi}_- , \tag{3.36}$$

$$E_{yy} = -(sc_0/\sigma)\partial_x \Phi , \tag{3.37}$$

$$E_{zy} = -\mu_0 \partial_x \dot{\Pi}_+ - (cc_0/\sigma)\partial_x \Phi ; \tag{3.38}$$

$\hat{\mathbf{m}} = \hat{\mathbf{z}}$:

$$E_{xz} = +\mu_0 \partial_{y_0} \dot{\Pi}_- , \tag{3.39}$$

$$E_{yz} = +\mu_0 \partial_x \dot{\Pi}_- + (ss_0/\sigma)\partial_x \Phi , \tag{3.40}$$

$$E_{zz} = +(cs_0/\sigma)\partial_x \Phi , \tag{3.41}$$

with Φ given in (3.12). For computing E_{xy} and E_{xz} we have used the identities

$$\mu_0 \sigma(\partial_z \dot{\Pi}_+ + \partial_{z_0} \dot{\Pi}_-) + c_0[\partial_y(s\Phi) + \partial_z(c\Phi)] = 0 , \tag{3.42}$$

$$\mu_0 \sigma(\partial_y \dot{\Pi}_- + \partial_{y_0} \dot{\Pi}_-) + s_0[\partial_y(s\Phi) + \partial_z(c\Phi)] = 0 . \tag{3.43}$$

Straightforward differentiaton using (3.23) yields

$$\mathbf{E}(\mathbf{r}|\,\mathbf{r}_0;\, t) = \mathscr{E}(\mathbf{r}|\,\mathbf{r}_0;\, t)\,\hat{\mathbf{m}} \tag{3.44}$$

with

$$\mathscr{E} = w_- \mathscr{E}_- + w_+ \mathscr{E}_+ + \mathscr{F} , \tag{3.45}$$

where the diffraction tensors $\mathscr{E}_\pm$ and $\mathscr{F}$ are now given by

$$\mathscr{E}_\pm = q_\pm \cdot \begin{pmatrix} 0 & -\zeta_\pm & \mp\eta \\ \zeta_\pm & 0 & \pm\xi \\ -\eta & \xi & 0 \end{pmatrix} , \tag{3.46}$$

$$\mathscr{F} = \bar{q} \cdot \begin{pmatrix} 0 & r\,s\,c_0 & -r\,s\,s_0 \\ r_0\,s\,c_0 & \xi\,s\,c_0 & -\xi\,s\,s_0 \\ r_0\,c\,c_0 & \xi\,c\,c_0 & -\xi\,c\,s_0 \end{pmatrix} \tag{3.47}$$

with

$$q_\pm = -\frac{m_0 \cdot \exp[-R_\pm^2/(4\tau)]}{16\sigma\sqrt{\pi^3\tau^5}} , \quad \bar{q} = -\frac{m_0 \cdot \exp[-\bar{R}^2/(4\tau)]}{8\sigma\pi^2\tau^2\sqrt{r\,r_0}} . \tag{3.48}$$

The first column of the diffraction tensors gives the Cartesian electric field components for a source dipole in the x-direction. Similarly, the second and third columns refer to dipoles in the y- and z-directions, respectively. The alternative product representation of the edge diffraction term,

$$\mathscr{F} = \bar{q} \cdot \mathrm{diag}(s, s, c) \begin{pmatrix} 0 & r & -r \\ r_0 & \xi & -\xi \\ r_0 & \xi & -\xi \end{pmatrix} \mathrm{diag}(c_0, c_0, s_0) , \tag{3.49}$$

shows that the corresponding horizontal electric field vanishes at $\varphi = 0$ and $\varphi = 2\pi$, whereas surface charges on the sheet cause a discontinuity of the vertical electric component across the sheet. The electric field components resulting from the source and its mirror image exhibit the same behaviour.

At the edge, the electric field shows the singular behaviour postulated by the edge conditions (2.9). The broken symmetry in the diagonal elements of the diffraction tensors is remarkable: whereas these elements are missing in source and image source, edge diffraction creates E_{yy} and E_{zz}, but does not affect E_{xx}. Therefore, the dipole in the x-direction has much in common with the TM polarization, where the current flow is confined to the plane perpendicular to the strike direction.

All tensor elements, except E_{xx}, show a uniform late-time behaviour: the elements of $\mathscr{E}_\pm$ decay as $t^{-5/2}$ and the elements of $\mathscr{F}$ as t^{-2}, such that the late-time behaviour of $\mathbf{E}$ is dominated by edge diffraction. This is illustrated in Fig. 3 by the current flow induced by a dipole in the x-direction, where according to (3.33)–(3.35) the current density can be represented as

$$\mathbf{J} = \nabla \times (\hat{\mathbf{x}} S) \quad \text{with} \quad S := -\mu_0 \sigma \dot{\Pi}_+ . \tag{3.50}$$

The function S plays the role of a current function. Therefore, the streamlines in the (y, z)-plane are given by the isolines $S = \text{const}$. In Fig. 3 six snapshots are shown of the current flow in the (y, z)-plane induced when an x-dipole at position $\times$ was shut off at $t = 0$. The parameter given is the dimensionless

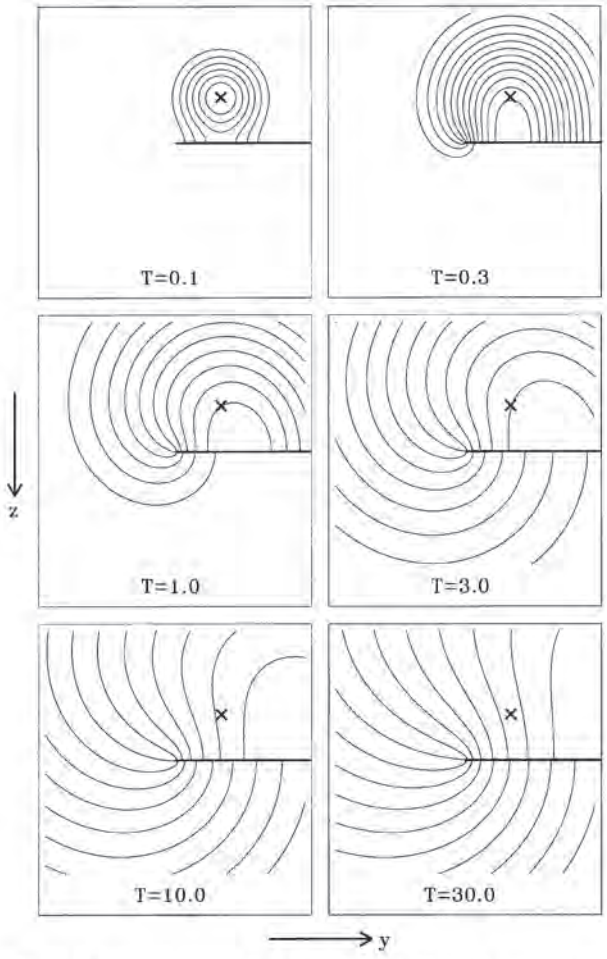

Figure 3. Lines of current flow for a dipole in the x-direction in the plane $x = x_0$. At early time (upper two panels) the current is dominated by the source geometry and flows in the clockwise direction as the current prior to shut-off. At late time (lower two panels) the current geometry is controlled by the slowly decaying edge-current system. The current lines leave the half-plane at its tip. The current flowing between adjacent lines decreases with time [$T = t/(\mu_0 \sigma r_0^2)$].

time $T:=t/(\mu_0\sigma r_0^2)$. Prior to shut-off, the x-dipole can be represented by a concentrated clockwise current flow at $\times$. The two snapshots at the top represent the early-time regime, where the pattern of current flow is dominated by the source current, which—in accordance with Lenz' rule—continues to flow in the direction of the current prior to shut-off. For $T=0.1$ the current flow is still confined to a small region, but current lines start to be short-circuited by the perfectly conducting half-plane. For $T=0.3$ the edge current system starts to develop. The two snapshots in the centre are representative for the intermediate-time regime, where the geometry of the original current system is still visible, but the edge current system starts to fill the space. In the late-time regime (bottom) the source current structure is barely visible in the flow pattern and the edge current system dominates. In this regime, all current lines shown leave the half-plane and return to it far to the right at the upper side of the half-plane (where the memory of the source geometry is still present).

The density of the surface charges accumulated at the half-plane is shown in Fig. 4 for the three orientations of the dipole with snapshots representative of the early-time and intermediate-time regimes. The source is at the same position as in Fig. 3; however, the projection of the source point onto the (x, y)-plane is marked. Regions of different polarity are separated by thick lines. Positive charges are present where current lines leave the half-plane. For the x-dipole, the charge distribution pattern is easily reconciled with the current flow shown in Fig. 3. For the z-dipole, the clockwise horizontal source current system in the (x, y)-plane drives positive charges to the edge for $\xi<0$ and removes them for $\xi>0$. These charges do not immediately reflect the source structure and are confined to the neighbourhood of the edge at early time. At late time, the charge pattern approaches that of the y-dipole (apart from the sign). For the three dipole orientations the charge density $\sigma_e=\epsilon[E_z(z=0^+)-E_z(z=0^-)]$ in $y>0$, $z=0$ is given by

$$\sigma_{ex}=+2\epsilon[q\eta\ \mathrm{erf}(c_0\sqrt{rr_0/\tau})-\bar{q}r_0c_0], \tag{3.51}$$

$$\sigma_{ey}=-2\epsilon\xi[q\ \mathrm{erf}(c_0\sqrt{rr_0/\tau})+\bar{q}c_0], \tag{3.52}$$

$$\sigma_{ez}=+2\epsilon\xi\bar{q}s_0, \tag{3.53}$$

where

$$q:=-\frac{m_0\cdot\exp[-R^2/(4\tau)]}{16\sigma\sqrt{\pi^3\tau^5}},\quad R^2:=\xi^2+\eta^2+z_0^2 \tag{3.54}$$

and $\bar{q}$ is defined by (3.48) with $r=y$.

4 THE TRANSIENT RESPONSE INCLUDING DISPLACEMENT CURRENTS

4.1 The complete potentials in the time domain

As extensions of the quasi-static fields $\dot{P}_\pm$, Φ and $\dot{\Phi}$ (given in eqs 3.6, 3.12 and 3.13) we require now their complete form as Fourier transforms of $\tilde{P}_\pm$ and $\tilde{\Phi}$, where k is used in its full form (2.7) including the displacement currents.

For notational convenience, distance and time are normalized by the intrinsic scales ℓ and γ, which are defined by the electromagnetic properties of the medium as

$$\ell:=\frac{2}{\sigma}\sqrt{\frac{\epsilon}{\mu_0}},\quad \gamma:=\frac{2\epsilon}{\sigma}. \tag{4.1}$$

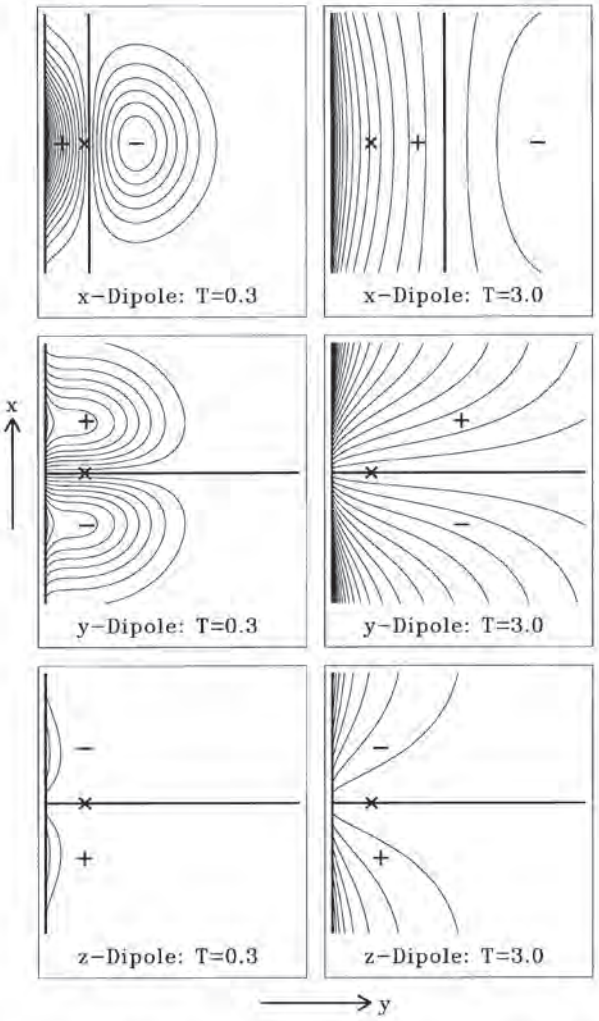

Figure 4. Surface charge density induced in the half-plane by the three orientations of dipoles at early and intermediate time. The cross ($\times$) marks the projection of the source shown in Fig. 3 onto the half-plane. Current lines leave the half-plane at regions with positive charge density ($+$). For a given time T, the charge density between adjacent isolines differs for the three orientations by the same amount.

These scales imply a scaling velocity $v:=\ell/\gamma=1/\sqrt{\epsilon\mu_0}$. In a lossy medium, the dispersive velocity of light increases with frequency and tends for high frequencies to the asymptotic value v, which is the velocity of the first arrivals of the signal; v is equivalent to the velocity of light in an *insulating* medium with permittivity ϵ. The time $\gamma/2$ is the decay time of free charges in a uniform full space with conductivity σ and permittivity ϵ. In a typical geophysical medium with $\sigma=10^{-2}$ S m^{-1} and $\epsilon=9\epsilon_0=8\times10^{-11}$ F m^{-1} we obtain with $\mu_0=4\pi\times10^{-7}$ H m^{-1} the scales $\ell=1.6$ m, $\gamma=1.6\times10^{-8}$ s and $v=10^8$ m s^{-1}.

If R is the generic distance between source and receiver and t the time elapsed since shut-off, the non-dimensional quantities a and b used in the following are defined as

$$a:=\frac{R}{\ell},\quad b:=\frac{t}{\gamma}. \tag{4.2}$$

a can also be considered as the first arrival traveltime R/v normalized with γ.

The basic Fourier transforms required are

$$\frac{1}{2\pi}\int_{-\infty}^{+\infty} K_0(kR)\,\mathrm{e}^{i\omega t}\,d\omega = \frac{\mathrm{e}^{-b}}{\gamma}\cdot\frac{\cosh\sqrt{b^2-a^2}}{\sqrt{b^2-a^2}}\cdot\Theta(b-a)\,, \quad (4.3)$$

$$\frac{1}{2\pi}\int_{-\infty}^{+\infty} \mathrm{e}^{-kR+i\omega t}\,d\omega = \frac{\mathrm{e}^{-b}}{\gamma}\cdot\left[\delta(b-a)+a\,\frac{I_1(\sqrt{b^2-a^2})}{\sqrt{b^2-a^2}}\cdot\Theta(b-a)\right], \quad (4.4)$$

where $\Theta(\cdot)$ is the Heaviside unit function, $\delta(\cdot)$ the Dirac δ-function and $I_1(\cdot)$ the modified Bessel function of the first kind and first order. With additional factors $1/(2\pi)$ and $1/(4\pi R)$, these identities are the well-known 2-D and 3-D scalar Green's functions of the wave equation in a lossy medium (e.g. Chew 1990, pp. 232–235; Morse & Feshbach 1953, pp. 865–869). For a direct evaluation of the integrals, the contour in the ω-plane is contracted for $t > R/v$ around the branch cut from $\omega=0$ to $\omega=i\sigma/\epsilon$. The resulting simpler integrals are found in tables.

The quasi-static regime is reached if $t \gg \max(R/v, \gamma)$, which is equivalent to $b \gg \max(a, 1)$. Then

$$\mathrm{e}^{-b}\cosh\sqrt{b^2-a^2} \simeq \frac{1}{2}\exp\left(-\frac{a^2}{2b}\right),$$
$$\mathrm{e}^{-b} I_1(\sqrt{b^2-a^2}) \simeq \frac{1}{\sqrt{2\pi b}}\exp\left(-\frac{a^2}{2b}\right), \quad (4.5)$$

such that (4.3) and (4.4) reduce to

$$\frac{1}{2\pi}\int_{-\infty}^{+\infty} K_0(kR)\,\mathrm{e}^{i\omega t}\,d\omega \simeq \frac{1}{2t}\exp\left(-\frac{\mu_0\sigma R^2}{4t}\right), \quad (4.6)$$

$$\frac{1}{2\pi}\int_{-\infty}^{+\infty} \mathrm{e}^{-kR+i\omega t}\,d\omega \simeq \sqrt{\frac{\mu_0\sigma R^2}{4\pi t^3}}\exp\left(-\frac{\mu_0\sigma R^2}{4t}\right), \quad (4.7)$$

which are in agreement with the quasi-static transforms (3.5) and (3.11). The quasi-static early time is defined by $\mu_0\sigma R^2/t = 2a^2/b = 2a(a/b) > 1$. In view of $a/b \ll 1$ this regime can be reached only for $a \gg 1$.

The presentation of potentials and fields is greatly simplified by the introduction of two sets of functions. The first set is recursively defined by

$$f_{n+1}(x) = \frac{1}{x}\cdot\frac{d f_n(x)}{d x} \quad (4.8)$$

and starts with

$$f_0(x) = \cosh x/x\,, \quad (4.9)$$

$$f_1(x) = [x\sinh x - \cosh x]/x^3\,, \quad (4.10)$$

$$f_2(x) = [(x^2+3)\cosh x - 3x\sinh x]/x^5\,, \quad (4.11)$$

$$f_3(x) = [(x^3+15x)\sinh x - (6x^2+15)\cosh x]/x^7\,. \quad (4.12)$$

These functions can be represented by modified Bessel functions of order $\nu = -(n+1/2)$, $f_n(x) = \sqrt{\pi/2}\,x^\nu I_\nu(x)$ (see Abramowitz & Stegun 1972, eqs 10.2.14 and 9.6.28). The second set is simply

$$g_n(x) := x^{-n}\cdot I_n(x)\,, \quad (4.13)$$

which also satisfies the recurrence relation (4.8) (see Abramowitz & Stegun 1972, eq. 9.6.28), i.e.

$$g_{n+1}(x) = \frac{1}{x}\cdot\frac{d g_n(x)}{d x}\,. \quad (4.14)$$

Moreover, f_n and g_n satisfy the recurrence relations

$$x^2 f_{n+1} + (2n+1) f_n - f_{n-1} = 0\,, \quad x^2 g_{n+1} + 2n g_n - g_{n-1} = 0\,. \quad (4.15)$$

For the calculation of $\dot{P}_\pm$ we introduce the abbreviations

$$\bar{a} := \frac{\bar{R}}{\ell}\,, \quad a_\pm := \frac{R_\pm}{\ell}\,, \quad v_\pm := \sqrt{b^2-a_\pm^2} \geq 0\,,$$
$$\mu_\pm := a_\pm \sinh u_\pm = \frac{2\sqrt{r r_0}}{\ell}\cos\frac{\alpha_\pm}{2}\,, \quad (4.16)$$

implying $\bar{a} = \sqrt{a_\pm^2 + \mu_\pm^2} = a_\pm\cosh u_\pm$.

Depending on the point of observation, four different situations have to be distinguished for a given time. As an illustration, Fig. 5 shows a snapshot of the wave fronts of the primary, reflected and diffracted waves at a very early time, shortly after the primary wave has hit the edge. The spherical primary wave, emanating from $\mathbf{r}_0$, vanishes for $R_- > vt$ (or $a_- > b$) and in the shadow zone $\cos(\alpha_-/2) < 0$ (or $\mu_- < 0$). The reflected wave arises when the primary wave reaches the half-plane (or its extension in $y < 0$) and can be presented by a spherical wave emitted from the image source at $\bar{\mathbf{r}}_0$. In the context of the reflected wave, a region is called 'illuminated' if it can be reached by the reflected wave, that is, if the image source is *invisible*. Correspondingly, in a 'shadow' region the image source is visible (region $\mu_+ < 0$ in Fig. 5). The diffracted wave, resembling a cylindrical wave, is excited at the edge after the primary wave has arrived. It merges at the boundaries $\mu_- = 0$

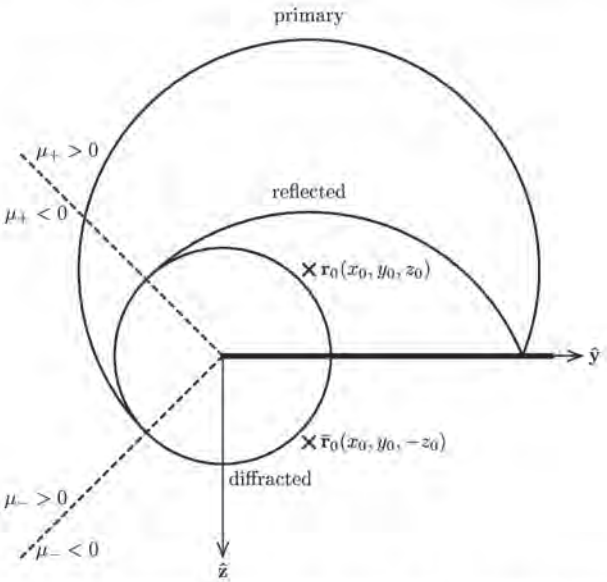

Figure 5. The system of wave fronts shortly after the primary wave has hit the edge. The dashed lines mark the boundary between light and shadow of source ($\mu_- = 0$) and image source ($\mu_+ = 0$) (see Fig. 2). Except at the points where the diffracted wave coalesces with the primary or reflected wave, they are not associated with field singularities (see Fig. 7).

and $\mu_+ = 0$ with the primary and reflected waves, respectively. Only the diffracted wave exists in $\mu_- < 0$. In regions affected by the diffracted wave, it is the superposition of primary, reflected and diffracted wave components that gives a continuous field across the boundaries $\mu_\pm = 0$. Since the wave front spreads out with the velocity of light, in practice almost all geophysical observations are made in the diffractive regime. For $P_\pm$ at a fixed point, the following four time windows, (a), (b_1), (b_2) and (c), have to be considered.

(a) $0 < b < a_\pm$

The primary (a_-) or reflected (a_+) wave has not yet arrived at the point of observation. Consequently,

$$\dot P_\pm = 0 . \tag{4.17}$$

(b) $a_\pm \le b < \bar a$ or $|\mu_\pm| > v_\pm \ge 0$

In this time window, the diffracted wave, resulting from the interaction of the primary wave with the edge, has not yet arrived (normalized first-arrival traveltime $\bar a$). However, the primary and reflected waves are present in the illuminated region ($\mu_\pm > 0$), but absent in the shadow region ($\mu_\pm < 0$). More precisely, in regions where the reflected wave can exist, it is always preceded by the primary wave. Therefore, two subcases have to be distinguished.

(b_1) $a_- \le b < a_+ < \bar a$ and $\mu_- > 0$: only the primary wave is present ($\dot P_- \ne 0$, $\dot P_+ = 0$);

(b_2) $a_- < a_+ \le b < \bar a$ and $\mu_\pm > 0$: primary and reflected waves are present ($\dot P_\pm \ne 0$). With the uniform full-space potential in the frequency domain,

$$\tilde P_\pm = \frac{\tilde m \cdot \exp(-kR_\pm)}{4\pi R_\pm} , \tag{4.18}$$

we obtain from (4.4)

$$\dot P_\pm = -\frac{m_0\, \mathrm{e}^{-b}}{4\pi\gamma\ell}\left[\frac{\delta(b-a_\pm)}{a_\pm} + g_1(v_\pm)\cdot\Theta(b-a_\pm)\right]\cdot\Theta(\mu_\pm),$$
$$|\mu_\pm| > v_\pm \ge 0 . \tag{4.19}$$

In the illuminated region, the first arrival has the sharp signature of a spherical wave. However, the amplitude is (strongly) damped by the factor $\mathrm{e}^{-b} = \mathrm{e}^{-a_\pm}$, such that it decays with the scale length ℓ. The second part is built up by the slower low-frequency components and merges for late time into the diffusive quasi-static limit with its $t^{-3/2}$ decay. For simplicity, the form of $\dot P_\pm$ in (4.19) has been derived by physical arguments. However, it also follows rigorously from the integral representation (4.20) given below.

(c) $b > \bar a$ or $|\mu_\pm| < v_\pm$

This is the principal time window, in which the diffracted field originating from the edge is also present. Using the relation $K_1(\cdot) = -K_0'(\cdot)$ and eqs (3.4), (3.3), (2.15), (2.16), (4.4) and (4.4), we obtain with $\alpha := a_\pm \cosh u$

$$\dot P_\pm = -\frac{m_0\, \mathrm{e}^{-b}}{4\pi\gamma\ell}\left\{\frac{I_1(v_\pm)}{2v_\pm} - \frac{1}{\pi}\int_0^{\mu_\pm}\frac{\partial}{\partial\alpha}\left[\frac{\cosh\sqrt{b^2-\alpha^2}}{\sqrt{b^2-\alpha^2}}\cdot\Theta(b-\alpha)\right]du\right\}. \tag{4.20}$$

Since $b > \bar a = a_\pm \cosh u_\pm$, we have in the whole range of integration $\Theta(b-\alpha) = 1$. Therefore, the new variables and abbreviations,

$$\mu := a_\pm \sinh u , \quad \kappa_\pm := \sqrt{v_\pm^2 - \mu^2} , \tag{4.21}$$

yield

$$\dot P_\pm = -\frac{m_0\, \mathrm{e}^{-b}}{8\pi\gamma\ell}\left[g_1(v_\pm) + \frac{2}{\pi}\int_0^{\mu_-} f_1(\kappa_\pm)\, d\mu\right], \quad |\mu_\pm| < v_\pm , \tag{4.22}$$

where $f_1(\cdot)$ and $g_1(\cdot)$ are defined above. For $b \to \bar a$ (or $|\mu_\pm| \to v_\pm$), the potential $\dot P_\pm$ with

$$\dot P_\pm \simeq \frac{m_0\, \mathrm{e}^{-b}}{4\pi^2\gamma\ell\mu_\pm\sqrt{b^2-\bar a^2}} \tag{4.23}$$

shows the typical wake pattern of a 2-D edge wave.

The presentation of fields in the diffractive regime is further simplified by introducing the abbreviation

$$h_n^\pm := g_n(v_\pm) + \frac{2}{\pi}\int_0^{\mu_-} f_n(\kappa_\pm)\, d\mu . \tag{4.24}$$

Then,

$$\dot P_\pm = -\frac{m_0\, \mathrm{e}^{-b}}{8\pi\gamma\ell}\cdot h_1^\pm , \quad |\mu_\pm| < v_\pm . \tag{4.25}$$

The contribution of the time-harmonic potential $\tilde\Phi$ to the transient electric and magnetic fields is described by the functions Ψ and $\dot\Phi$, respectively, and is present only in the diffractive regime. From (2.37), (2.7), (3.3) and (4.3), with $\lambda := \sqrt{b^2-\bar a^2}$ for $b > \bar a$,

$$\Psi = \frac{1}{2\pi}\int_{-\infty}^{+\infty}\frac{\tilde\Phi}{\sigma + i\omega\epsilon}\,\mathrm{e}^{i\omega t}\, d\omega = -\frac{m_0\mu_0\, \mathrm{e}^{-b}}{2\pi^2\gamma\sqrt{rr_0}}\cdot f_0(\lambda) , \tag{4.26}$$

$$\dot\Phi = \frac{1}{2\pi}\int_{-\infty}^{+\infty} i\omega\tilde\Phi\,\mathrm{e}^{i\omega t}\, d\omega = \frac{\sigma}{2\gamma}\,\partial_b(2+\partial_b)\Psi$$
$$= \frac{m_0\, \mathrm{e}^{-b}}{2\pi^2\gamma\ell^2\sqrt{rr_0}}\,[2f_1(\lambda) - \bar a^2 f_2(\lambda)] , \tag{4.27}$$

where we have used $\partial_b f_n(\lambda) = b f_{n+1}(\lambda)$, (4.15) and $\mu_0\sigma = 2\gamma/\ell^2$. In the quasi-static limit, Ψ corresponds to Φ/σ.

4.2 Explicit expressions for the transient electromagnetic field

After having established the transient form of the potentials, we are in a position to determine the corresponding electromagnetic field. Compared with (3.14)–(3.22) and (3.33)–(3.41), formally only a few modifications are required. For instance, for $\hat{\mathbf{m}} = \hat{\mathbf{y}}$ the field components are

$$\dot H_{xy} = -\partial_{xy_0}\dot\Pi_+ , \tag{4.28}$$

$$\dot H_{yy} = -[\partial_{yy_0} + \mu_0\partial_t(\sigma + \epsilon\partial_t)]\dot\Pi_+ - c\, c_0\,\dot\Phi$$
$$= -[\partial_{yy_0} + \ell^{-2}\partial_b(2+\partial_b)]\dot\Pi_+ - c\, c_0\,\dot\Phi , \tag{4.29}$$

$$\dot H_{zy} = -\partial_{zy_0}\dot\Pi_+ + s\, c_0\,\dot\Phi , \tag{4.30}$$

$$E_{xy} = -\mu_0\partial_{z_0}\dot\Pi_- , \tag{4.31}$$

$$E_{yy} = -sc_0\partial_x\Psi , \tag{4.32}$$

$$E_{zy} = -\mu_0\partial_x\dot\Pi_+ - cc_0\partial_x\Psi . \tag{4.33}$$

Let

$$\dot{\mathbf{H}}(\mathbf{r}|\,\mathbf{r}_0;\,t)=\dot{\mathscr{H}}(\mathbf{r}|\,\mathbf{r}_0;\,t)\,\hat{\mathbf{m}}\quad\text{with}\quad\dot{\mathscr{H}}=\dot{\mathscr{H}}_-+\dot{\mathscr{H}}_++\dot{\mathscr{D}}\,. \tag{4.34}$$

Then the diffraction tensors $\dot{\mathscr{H}}_\pm$ and $\dot{\mathscr{D}}$ read in the principal time window $b>\bar{a}$

$$\dot{\mathscr{H}}_\pm=p_\pm\cdot\begin{pmatrix}\xi^2+\Delta_\pm & \xi\eta & \mp\xi\zeta_\pm\\ \xi\eta & \eta^2+\Delta_\pm & \mp\eta\zeta_\pm\\ \xi\zeta_\pm & \eta\zeta_\pm & \mp(\zeta_\pm^2+\Delta_\pm)\end{pmatrix}, \tag{4.35}$$

and

$$\dot{\mathscr{D}}=\bar{p}\cdot\begin{pmatrix}0 & \xi r\,c\,c_0 & -\xi r\,c\,s_0\\ -\xi r_0\,c\,c_0 & \Delta\,c\,c_0 & -(\Delta+r_0^2+rr_0)\,c\,s_0\\ \xi r_0\,s\,c_0 & -(\Delta+r^2+rr_0)\,s\,c_0 & (\Delta+r^2+r_0^2)\,s\,s_0\end{pmatrix}, \tag{4.36}$$

with

$$\Delta_\pm:=\ell^2(h_1^\pm-2h_2^\pm-b^2\,h_3^\pm)/h_3^\pm\,, \tag{4.37}$$

$$\Delta:=r^2\cos\varphi+r_0^2\cos\varphi_0-\bar{R}^2+3\ell^2 f_1(\lambda)/[2f_2(\lambda)]\,, \tag{4.38}$$

$$p_\pm:=-\frac{m_0\,\mathrm{e}^{-b}}{8\pi\gamma\ell^5}\cdot h_3^\pm\,,\quad \bar{p}:=-\frac{m_0\,\mathrm{e}^{-b}}{2\pi^2\gamma\ell^4\sqrt{rr_0}}\cdot f_2(\lambda)\,, \tag{4.39}$$

where $h_n^\pm$ is defined in (4.24) and $\lambda^2=b^2-\bar{a}^2=(t/\gamma)^2-(\bar{R}/\ell)^2$. Moreover, let

$$\mathbf{E}(\mathbf{r}|\,\mathbf{r}_0;\,t)=\mathscr{E}(\mathbf{r}|\,\mathbf{r}_0;\,t)\,\hat{\mathbf{m}}\quad\text{with}\quad\mathscr{E}=\mathscr{E}_-+\mathscr{E}_++\mathscr{F}. \tag{4.40}$$

Then the diffraction tensors $\mathscr{E}_\pm$ and $\mathscr{F}$, differing from the quasi-static case only by the pre-multipliers, are given by

$$\mathscr{E}_\pm=q_\pm\cdot\begin{pmatrix}0 & -\zeta_\pm & \mp\eta\\ \zeta_\pm & 0 & \pm\xi\\ -\eta & \xi & 0\end{pmatrix}, \tag{4.41}$$

$$\mathscr{F}=\bar{q}\cdot\begin{pmatrix}0 & r\,s\,c_0 & -r\,s\,s_0\\ r_0\,s\,c_0 & \xi\,s\,c_0 & -\xi\,s\,s_0\\ r_0\,c\,c_0 & \xi\,c\,c_0 & -\xi\,c\,s_0\end{pmatrix}, \tag{4.42}$$

with

$$q_\pm:=-\frac{m_0\mu_0\,\mathrm{e}^{-b}}{8\pi\gamma\ell^3}\cdot h_2^\pm\,,\quad \bar{q}:=-\frac{m_0\mu_0\,\mathrm{e}^{-b}}{2\pi^2\gamma\ell^2\sqrt{rr_0}}\cdot f_1(\lambda)\,. \tag{4.43}$$

With the present notation we try to give the most concise presentation of the fields under the inclusion of displacement currents. Therefore, correspondences with the quasi-static case may be masked. For example, the present quantities $\dot{\mathscr{H}}_\pm$ and $p_\pm$ correspond in the quasi-static usage to $w_\pm\cdot\mathscr{H}_\pm$ and $w_\pm\cdot p_\pm$. The same holds for $\mathscr{E}_\pm$ and $q_\pm$. Also, $\dot{\mathscr{D}}_{xx}=0$ in the present case, whereas in the quasi-static usage $\mathscr{D}_{xx}\neq 0$. In fact, this (regular) contribution is now included in $(\dot{\mathscr{H}}_-+\dot{\mathscr{H}}_+)_{xx}$. Similar observations apply to the two other diagonal elements of $\dot{\mathscr{D}}$. However, Δ, $\bar{p}$, and $\bar{q}$ merge into their quasi-static counterparts.

Numerical stability in the late-time regime is achieved by amalgamating the exponentially small factor e^{-b} with the exponentially large factors f_n and g_n, e.g.

$$2\,\mathrm{e}^{-b}\cosh\sqrt{b^2-a^2}=\exp[-a^2/(b+\sqrt{b^2-a^2})]+\exp[-(b+\sqrt{b^2-a^2})]. \tag{4.44}$$

The functions g_n are treated similarly by using the modified Bessel functions in their scaled version $I_n(x)\,\mathrm{e}^{-x}$, which is also given in most special function packages.

The preceding results hold in the principal time window $b>\bar{a}$. In the window $a_\pm<b<\bar{a}$, where the diffracted wave has not yet arrived, the undisturbed primary (and reflected) field is present in the illuminated region, i.e. $\bar{p}=\bar{q}=0$ and

$$p_\pm:=-\frac{m_0\,\mathrm{e}^{-b}}{4\pi\gamma\ell^5}\cdot g_3(v_\pm)\cdot\Theta(\mu_\pm)\,,\qquad q_\pm:=-\frac{m_0\mu_0\,\mathrm{e}^{-b}}{4\pi\gamma\ell^3}\cdot g_2(v_\pm)\cdot\Theta(\mu_\pm)\,, \tag{4.45}$$

$$\Delta_\pm:=\ell^2[g_1(v_\pm)-2g_2(v_\pm)-b^2\,g_3(v_\pm)]/g_3(v_\pm) \tag{4.46}$$

$$=2\ell^2 g_2(v_\pm)/g_3(v_\pm)-R_\pm^2\,. \tag{4.47}$$

In the last step, $g_1(v_\pm)$ was eliminated on using (4.15). With the inclusion of displacement currents, the transient electromagnetic field of a magnetic dipole in a uniform lossy host was first derived by Wait (1953).

4.3 The transient current distribution

In this subsection the transition from propagation to diffusion is visualized by means of the current lines of a magnetic dipole in the x-direction, where the current flow is confined to the (y,z)-plane and the current density $\mathbf{J}$ can be derived from a current function by means of (3.50). We shall distinguish between the current function S_c for the conduction current and the current function S_t for the total current (including displacement currents). Confining our attention first to the primary field and putting for brevity $a:=|\mathbf{r}-\mathbf{r}_0|/\ell$, $v^2:=b^2-a^2$, we obtain with $\mu_0\sigma=2\gamma/\ell^2$, on using (4.19),

$$S_\mathrm{c}=-\mu_0\sigma\dot{P}_-=\frac{m_0\,\mathrm{e}^{-b}}{2\pi\ell^3}\left[g_1(v)\cdot\Theta(b-a)+\frac{\delta(b-a)}{a}\right], \tag{4.48}$$

$$S_\mathrm{t}=-\mu_0(\sigma\dot{P}_-+\epsilon\ddot{P}_-) \tag{4.49}$$

$$=\frac{m_0\,\mathrm{e}^{-b}}{4\pi\ell^3}\left[\{g_1(v)+b\,g_2(v)\}\cdot\Theta(b-a)+\left(\frac{1}{2}+\frac{1}{a}\right)\delta(b-a)+\frac{1}{a}\,\delta'(b-a)\right]. \tag{4.50}$$

When cylindrical coordinates (ϱ,ψ) are introduced with respect to the source point by

$$y-y_0=\varrho\cos\psi\,,\quad z-z_0=-\varrho\sin\psi\,, \tag{4.51}$$

the current flow is in the azimuthal direction and given according to (3.50) by $J_\psi=\partial_\varrho S$, where $\ell^2a^2=\xi^2+\varrho^2$. For $a<b$ the current flow is in the $-\psi$-direction, which is the direction of currents prior to shut-off. At the wave front $a=b$, the current becomes highly singular, showing a superposition of sheet currents with unipolar, dipolar and—in the case of displacement currents—quadrupolar structure. Since the singular

dipolar and quadrupolar currents are not associated with a net current flow, the unipolar sheet-current density in the ψ-direction is given by the jump of S,

$$S_c(a=b^+)-S_c(a=b^-)=-\frac{m_0\,e^{-b}}{4\pi\ell^3}\,,$$
$$S_t(a=b^+)-S_t(a=b^-)=-\frac{m_0\,e^{-b}}{8\pi\ell^3}\left[1+\frac{b}{4}\right]. \tag{4.52}$$

Due to the conductive host, the strength of the wave front $a=b$ exponentially decreases with the separation from the source. The scale length is ℓ. The current function of the image source is defined correspondingly and is superimposed on the primary current function according to Fig. 5.

In the diffractive regime $\bar{a}<b$ we put $S=S^-+S^+$, where according to (3.50) and (4.25),

$$S_c^\pm=-\mu_0\sigma\dot{P}_\pm=\frac{m_0\,e^{-b}}{4\pi\ell^3}\cdot h_1^\pm\,, \tag{4.53}$$

$$S_t^\pm=-\mu_0(\sigma\dot{P}_\pm+\epsilon\ddot{P}_\pm)=\frac{m_0\,e^{-b}}{8\pi\ell^3}\,[h_1^\pm+b\,h_2^\pm], \tag{4.54}$$

with $h_n^\pm$ defined in (4.24). Enhanced current flow occurs when approaching the diffractive wave front $\bar{a}=b$. From (4.53) and (4.54) it follows for $\bar{a}\to b$ that

$$S_c^\pm\simeq-\frac{m_0\,e^{-b}}{2\pi^2\ell^3\mu_\pm\sqrt{b^2-\bar{a}^2}}\,,\quad S_t^\pm\simeq+\frac{m_0\cdot b\cdot e^{-b}}{4\pi^2\ell^3\mu_\pm\sqrt{b^2-\bar{a}^2}^3}\,, \tag{4.55}$$

yielding singular current densities $\sim(b-\bar{a})^{-3/2}$ and $\sim(b-\bar{a})^{-5/2}$, respectively. The direction of the singular total current is opposite to that of the singular conduction current (see Fig. 7 below). Due to the 2-D nature of the diffractive wave front, the current density steadily increases towards $\bar{a}=b$ rather than being concentrated in the front as in the case of the spherical primary and reflected waves. These strong currents encountered for $\bar{a}\to b$ are balanced by the opposing concentrated sheet current (of infinite amplitude) at $\bar{a}=b$ that results when performing the differentiation $\partial_\alpha\Theta(b-\alpha)$ at $\alpha=a_\pm\cosh u_\pm=\bar{a}$ in (4.20).

At a given instant, the geometry of the current lines can be fixed by the two non-dimensional parameters

$$T:=\frac{t}{\mu_0\sigma r_0^2}\quad\text{and}\quad W:=\frac{vt}{r_0}\,, \tag{4.56}$$

quantifying, respectively, diffusion and wave propagation. The parameter T has already been used in Section 3.3. In terms of W and T the normalized distance of the source from the origin and the normalized time after shut-off are given by

$$a_0=\frac{r_0}{\ell}=\frac{W}{2T}\,,\quad b=\frac{t}{\gamma}=\frac{W^2}{2T}\,. \tag{4.57}$$

As pointed out in Section 4.1, the diffusive regime is reached for $b\gg\max(a_0,1)$.

Fig. 6 shows in the plane $x=x_0$ six snapshots of the conduction current lines for fixed T and varying W. The thick lines mark the fronts of the primary, reflected and diffracted waves that are associated with sheet currents. At the first snapshot, $W=0.5$, the wave front of the primary wave is midway between source point and edge; no interaction with the half-plane has taken place. This occurs at the next instant, $W=1$, where a

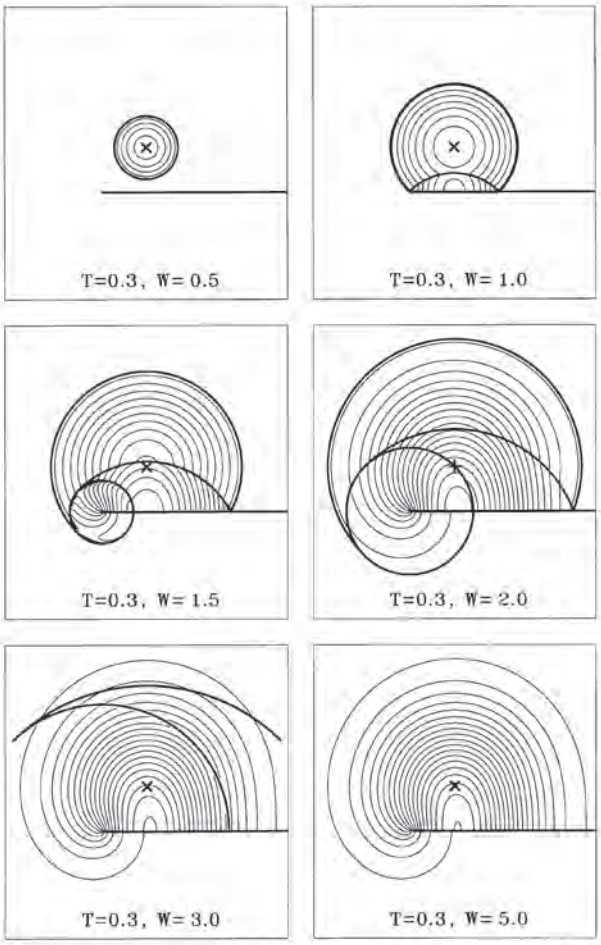

Figure 6. Conduction current lines in the plane $x=x_0$ for a dipole in the x-direction showing the transition from propagation to diffusion. The parameter $W=vt/r_0$ is the time elapsed since shut-off, normalized with the traveltime from the source to the edge. Moreover, $T=t/(\mu_0\sigma r_0^2)$ identifies the current system of Fig. 3, which is approached for $W\to\infty$. The cross ($\times$) denotes the source position $\mathbf{r}_0$ and the thick lines mark the wave fronts (see Fig. 5). In regions not affected by the diffracted wave, the current flows in the clockwise direction, with sheet currents flowing in the fronts. The amplitudes of these sheet currents decrease rapidly with time and are negligible for $W=3$. In the diffractive regime, the currents leave the half-plane at the tip. Close to the boundary of the diffraction circle, the geometry of current flow of the total current (including displacement currents) differs substantially from the conduction current flow (see Fig. 7).

reflected wave has emerged. The wave front just reaches the edge, and at the subsequent instant $W=1.5$ the diffracted wave has evolved. In the sequel, the radius of the diffraction circle steadily increases and the strength of the wave fronts strongly decreases in the conductive host as $\exp[-W^2/(2T)]$ such that e.g. for $W=3$ the current lines pass the reflected wave front almost unaffected. For $W=5$, the diffusive regime is reached in the section shown. The pattern of current lines agrees with that shown in Fig. 3 for $T=0.3$.

For an illustration of the different geometries of the conduction current and total current in the diffractive regime, the current lines in the diffraction circle are enlarged in Fig. 7 for

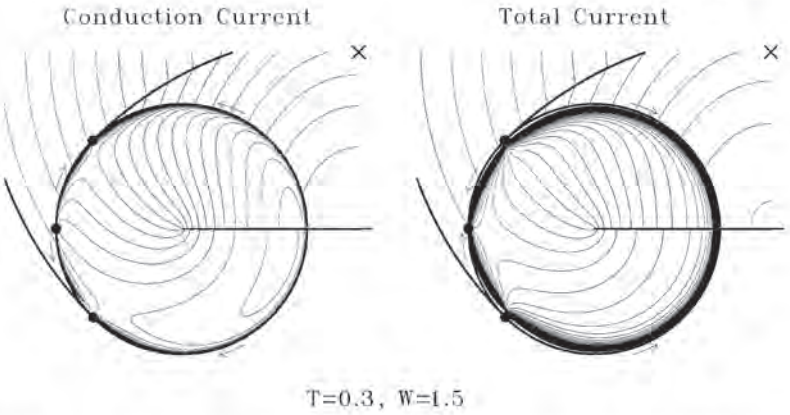

Figure 7. Enlarged presentation of the current flow of Fig. 6 for $W=vt/r_0=1.5$ for both the conduction current and the total current. The source point is marked by ×. The thick lines mark the fronts of Fig. 5. The points where the diffracted wave merges with the primary or reflected wave are points of diverging current flow inside the circle and convergent current flow on the circle for the conduction current. For the total current, the source nature is interchanged. Similar observations hold for the point $\varphi=\pi$ on the diffraction circle.

$vt/r_0=1.5$. As inferred from (4.55), the total current close to $\bar{a}=b$ is dominated by the displacement current with a polarity opposite to that of the conduction current. At the points marked by the dots, i.e. at $\varphi=\pi-\phi_0$, π and $\pi+\phi_0$, the singular current changes polarity. The arrows outside the diffraction circle mark the directions of the singular sheet currents, which balance the distributed currents of opposite direction inside the diffraction circle.

5 APPROXIMATE INCLUSION OF AN INSULATING AIR HALF-SPACE

The transient quasi-static full-space solution is distinguished by its extreme simplicity, which will be lost when turning our attention to the simplest model of geophysical relevance, where the perfectly conducting half-plane is embedded in a uniform half-space.

Although it is not difficult to design a numerical solution for this problem—and in the case of a horizontal half-plane even an analytical solution (see Appendix B)—in the spirit of this paper it is more desirable to obtain an approximate solution for a model including the air half-space by a modification of the full-space response.

The full-space field can be separated into a normal part consisting of the response of the uniform host and an anomalous part describing the effect of the half-plane. The simplest approximation consists of replacing the normal full-space response by the normal half-space response and retaining the anomalous full-space response as an approximation of the half-space.

The quality of this approximation is tested in a simple example shown in Fig. 8. We consider a horizontal half-plane at $z=0$, $y\geq 0$ with the air–earth interface at $z=-D$. In this interface a vertical magnetic dipole is placed at $\mathbf{r}_0=(0, y_0, -D)$ and the quasi-static transient vertical magnetic field component is measured at $\mathbf{r}=(0, y, -D)$. Let $R:=|\mathbf{r}-\mathbf{r}_0|=|y-y_0|$ and $\bar{y}=(y+y_0)/2$. The panel at the top left shows the normal fields. With $\beta:=R^2/(4\tau)$ we obtain from (3.27) for the full-space response

$$\dot{H}_{zzn}(\mathbf{r}|\,\mathbf{r}_0;\,t)=-\frac{m_0(1-\beta)\,\mathrm{e}^{-\beta}}{8\mu_0\sigma\sqrt{\pi^3\tau^5}}$$

$$=-\frac{m_0}{8\mu_0\sigma\sqrt{\pi^3\tau^5}}\,[1+\mathcal{O}(\beta)]\ \text{for}\ \beta\ll 1 \tag{5.1}$$

and from Spies & Frischknecht (1987, p. 297) for the half-space response

$$\dot{H}_{zzn}(\mathbf{r}|\,\mathbf{r}_0;\,t)$$

$$=\begin{cases}-\dfrac{m_0}{8\mu_0\sigma\sqrt{\pi^3\tau^5}}\left[\left(1+\dfrac{3}{2\beta}+\dfrac{9}{4\beta^2}\right)\mathrm{e}^{-\beta}-\dfrac{9\sqrt{\pi}\,\mathrm{erf}(\sqrt{\beta})}{8\sqrt{\beta^5}}\right]\\[2ex] -\dfrac{m_0}{20\mu_0\sigma\sqrt{\pi^3\tau^5}}\,[1+\mathcal{O}(\beta)]\ \text{for}\ \beta\ll 1\end{cases}. \tag{5.2}$$

Therefore, in the late-time regime ($\beta\ll 1$) the full-space response exceeds the half-space response by a factor 5/2 and in this regime a good approximation to the normal half-space field at time t is the full-space field at time $1.44\,t$.

According to (3.26), the anomalous diffraction tensor for the full space is given by

$$\dot{\mathcal{H}}_a=(-1+w_-)\dot{\mathcal{H}}_-+w_+\dot{\mathcal{H}}_++\dot{\mathcal{D}}\,, \tag{5.3}$$

with $\dot{\mathcal{H}}_\pm$ and $\dot{\mathcal{D}}$ defined in (3.27) and (3.28). Assuming that transmitter and receiver move with constant separation R along the y-axis, the resulting anomalous transient curves are displayed as thin lines for various midpoints $\bar{y}$ in the remaining five panels of Fig. 8 and compared with the anomalous half-space transients (thick lines). In general, the anomalous full-space response overestimates the anomalous half-space response. As in the case of the normal field, a better agreement would be obtained by relating the anomalous half-space transients at time t to the anomalous full-space transients at time $1.44\,t$.

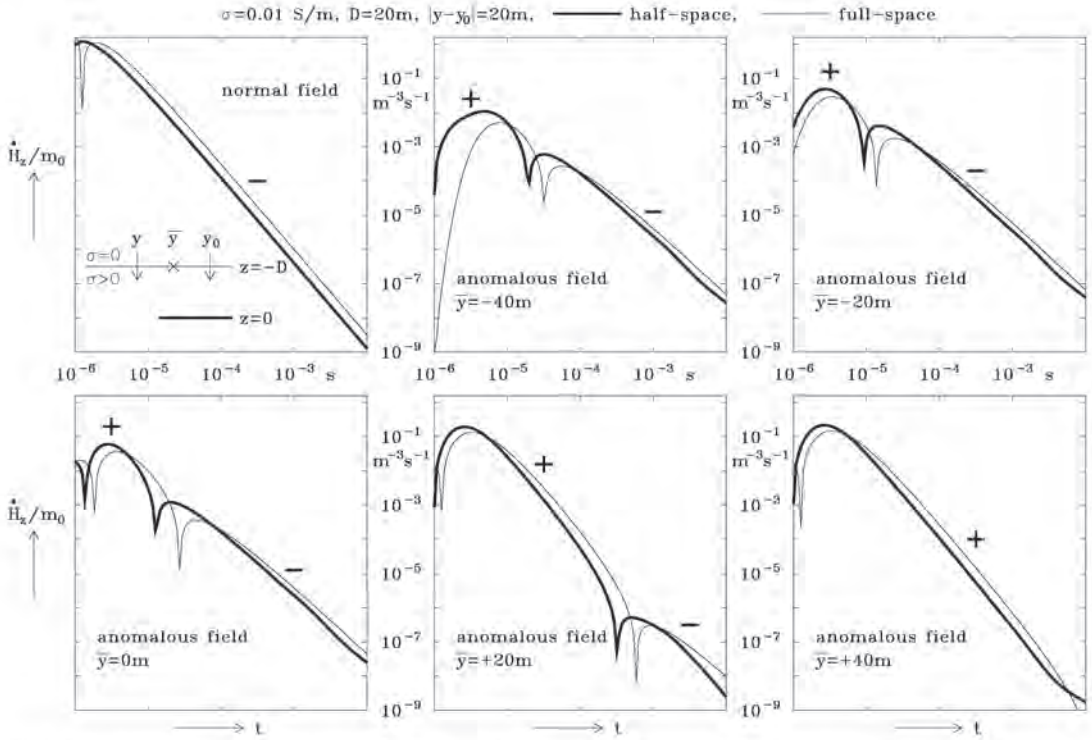

Figure 8. Half-plane decay curves for a full space (thin lines) and a half-space (thick lines) separated into a normal part (top left) and an anomalous part (remaining panels, different positions of the common-offset set-up). The cusps mark sign changes. After a time-shift, the anomalous full-space response may serve as an approximation for the anomalous half-space response, particularly in the late-time regime.

6 CONCLUDING REMARKS

The transient electromagnetic field of a perfectly conducting half-plane in a full space allows the simulation of quite complex fields despite its analytical simplicity. These fields might serve as easily accessible reference fields for numerical and geophysical studies. We have tried to present a complete coverage of the subject by always considering the full diffraction tensors of the scattered magnetic and electric fields, both in the quasi-static limit and in the wave domain. Attention has been confined to magnetic dipole sources. However, a brief treatment of grounded electric dipole sources is given in Appendix A, where the reciprocity theorem of Lorentz plays a fundamental role by relating the magnetic field of an electric dipole to the electric field of a magnetic dipole.

ACKNOWLEDGMENTS

My thanks go to David Johnson for stimulating my interest in the problem and to Gerhard Müller for drawing my attention to the transient scattering of seismic waves at a crack.

REFERENCES

Abramowitz, M. & Stegun, I.A., 1972. *Handbook of Mathematical Functions*, Dover, New York.

Born, M. & Wolf, E., 1983. *Principles of Optics*, Pergamon, Oxford.

Carlslaw, H.S. & Jaeger, J.C., 1963. *Operational Methods in Applied Mathematics*, Dover, New York.

Chew, W.C., 1990. *Waves and Fields in Inhomogeneous Media*, Van Nostrand & Reinhold, New York.

Clemmow, P.C., 1951. A method for the solution of a class of two-dimensional diffraction problems, *Proc. R. Soc. Lond.*, **A205,** 286–308.

Copson, E.T., 1950. Diffraction by a plane screen, *Proc. R. Soc. Lond.*, **A202,** 277–284.

Fertig, J. & Müller, G., 1979. Approximate diffraction theory for transparent half-planes with application to seismic-wave diffraction at coal seams, *J. Geophys.*, **46,** 349–367.

Grant, F.S. & West, G.F., 1965. *Interpretation Theory in Applied Geophysics*, McGraw-Hill, New York.

Hjelt, S.E., 1968. On the half-plane model in double-dipole electromagnetic prospecting, *Acta Polytech. Scand., Phys. Ser.*, **60,** 1–41.

Jones, D.S., 1950. Note on diffraction by an edge, *Quart. J. Mech. appl. Math.*, **3,** 420–434.

Jones, D.S., 1964. *The Theory of Electromagnetism*, Pergamon, Oxford.

Jones, D.S., 1986. *Acoustic and Electromagnetic Waves*, Oxford University Press, Oxford.

Macdonald, H.M., 1915. A class of diffraction problems, *Proc. Lond. math. Soc., Ser. 2*, **14,** 410–427.

Meixner, J., 1949. Die Kantenbedingung in der Theorie der Beugung elektromagnetischer Wellen an vollkommen leitenden ebenen Schirmen, *Ann. Phys., Ser. 6*, **6,** 2–9.

Morse, P.M. & Feshbach, H., 1953. *Methods of Theoretical Physics*, McGraw-Hill, New York.

Noble, B., 1958. Methods based on the Wiener-Hopf technique for the solution of partial differential equations, *Int. Ser. Monogr. Pure appl. Math.*, **7.**

Pao, Y.-H. & Mow, C.-C., 1973. *Diffraction of Elastic Waves and Dynamic Stress Concentrations*, Adam Hilger, London.

Pellerin, L., Labson, V.F. & Pfeifer, M.C., 1995. VETEM—a very early time electromagnetic system—the first year, *Proc. Symp. Application of Geophysics to Engineering and Environmental Problems (SAGEEP)*, 725–731.

Pellerin, L., Pfeifer, M.C. & Labson, V.F., 1996. VETEM—a very early time electromagnetic system—year 2, *Proc. Symp. Application of Geophysics to Engineering and Environmental Problems (SAGEEP)*, 91–95.

Senior, T.B.A., 1953. The diffraction of a dipole field by a perfectly conducting half-plane, *Q. J. Mech. appl. Math.*, **6**, 101–114.

Sommerfeld, A., 1896. Theorie der Diffraction, *Math. Ann.*, **47**, 317–374.

Sommerfeld, A., 1897. Über verzweigte Potentiale im Raum, *Proc. Lond. Math. Soc.*, **28**, 395–429.

Spies, B.R. & Frischknecht, F.C., 1987. Electromagnetic sounding, in *Electromagnetic Methods in Applied Geophysics*, vol. 2, pp. 285–425, ed. Nabighian, M.N., SEG, Tulsa, OK.

Vandakurov, Yu.V., 1954. Diffraction of electromagnetic waves—emitted from arbitrarily oriented electric or magnetic dipoles—at a perfectly conducting half-plane, *Zh. Eksp. Teor. Fiz.*, **26**, 3–18 (in Russian).

Wait, J.R., 1953. A transient magnetic dipole source in a dissipative medium, *J. appl. Physics*, **24**, 341–343.

Weidelt, P., 1983. The harmonic and transient electromagnetic response of a thin dipping dyke, *Geophysics*, **48**, 934–952.

Wesley, J.P., 1958. Response of a dyke to an oscillating dipole, *Geophysics*, **23**, 128–133.

West, G.F., 1960. Quantitative interpretation of electromagnetic prospecting measurements, *PhD thesis*, University of Toronto.

Williams, W.E., 1957. A note on the diffraction of a dipole field by a half-plane, *Q. J. Mech. appl. Math.*, **10**, 210–213.

Woods, B.D., 1957. The diffraction of a dipole field by a half-plane, *Q. J. Mech. appl. Math.*, **10**, 90–100.

APPENDIX A: THE QUASI-STATIC TRANSIENT ELECTRIC DIPOLE

After the detailed consideration of the magnetic dipole we shall cast a brief look at the quasi-static transient field of a grounded electric dipole, which can be derived from the field of a magnetic dipole.

The source is presented by the current moment $\mathbf{d}(t)$, which points from the negative towards the positive electrode with a modulus equal to the product of the electrode separation and the source current. The basic quasi-static equations in the frequency domain are

$$\nabla\times\tilde{\mathbf{H}}=\sigma\tilde{\mathbf{E}}+\tilde{\mathbf{d}}\delta(\mathbf{r}-\mathbf{r}_0)\,, \tag{A1}$$

$$\nabla\times\tilde{\mathbf{E}}=-i\omega\mu_0\tilde{\mathbf{H}}\,. \tag{A2}$$

With $k^2:=i\omega\mu_0\sigma$, the elimination of $\tilde{\mathbf{H}}$ then leads to

$$\nabla\times\nabla\times\tilde{\mathbf{E}}+k^2\tilde{\mathbf{E}}=-k^2(\tilde{\mathbf{d}}/\sigma)\delta(\mathbf{r}-\mathbf{r}_0)\,. \tag{A3}$$

Eq. (A3) has the same structure as (2.4), but because of different boundary conditions at the perfectly conducting half-plane, the electric field of an electric dipole is not related in a simple way to the magnetic field of a magnetic dipole. However, the magnetic field $\tilde{\mathbf{H}}^e(\mathbf{r}|\,\mathbf{r}_0)$ of an electric dipole is easily derived from the electric field $\tilde{\mathbf{E}}^m(\mathbf{r}_0|\,\mathbf{r})$ of a magnetic dipole by the Lorentz reciprocity theorem

$$-i\omega\mu_0\tilde{\mathbf{m}}\cdot\tilde{\mathbf{H}}^e(\mathbf{r}|\,\mathbf{r}_0)=\tilde{\mathbf{d}}\cdot\tilde{\mathbf{E}}^m(\mathbf{r}_0|\,\mathbf{r})\,, \tag{A4}$$

which holds in general non-uniform and anisotropic linear media, even with the inclusion of displacement currents. Assuming in the time domain the same excitation for both dipoles, i.e. $\tilde{\mathbf{m}}(\omega)=g(\omega)\mathbf{m}_0$ and $\tilde{\mathbf{d}}(\omega)=g(\omega)\mathbf{d}_0$ [e.g. $g(\omega)=-1/(i\omega)$ in the case of a sharp current shut-off], (A4) in the time domain reads

$$-\mu_0\mathbf{m}_0\cdot\dot{\mathbf{H}}^e(\mathbf{r}|\,\mathbf{r}_0;\,t)=\mathbf{d}_0\cdot\mathbf{E}^m(\mathbf{r}_0|\,\mathbf{r};\,t)\,. \tag{A5}$$

Let $\mathbf{d}_0=d_0\tilde{\mathbf{d}}$. Then, with (A5) we obtain for the magnetic field of an electric dipole from (3.44)–(3.48)

$$\dot{\mathbf{H}}^e(\mathbf{r}|\,\mathbf{r}_0;\,t)=\dot{\mathscr{H}}^e(\mathbf{r}|\,\mathbf{r}_0;\,t)\,\tilde{\mathbf{d}}\,, \tag{A6}$$

with

$$\dot{\mathscr{H}}^e=w_-\dot{\mathscr{H}}^e_-+w_+\dot{\mathscr{H}}^e_++\dot{\mathscr{D}}^e\,, \tag{A7}$$

where the diffraction tensors are given by

$$\dot{\mathscr{H}}^e_\pm=p_\pm\cdot\begin{pmatrix}0 & \pm\zeta_\pm & \eta\\ \mp\zeta_\pm & 0 & -\xi\\ \pm\eta & \mp\xi & 0\end{pmatrix}, \tag{A8}$$

$$\dot{\mathscr{D}}^e=\overline{p}\cdot\begin{pmatrix}0 & r\,c\,s_0 & r\,c\,c_0\\ r_0\,c\,s_0 & -\xi\,c\,s_0 & -\xi\,c\,c_0\\ -r_0\,s\,s_0 & +\xi\,s\,s_0 & +\xi\,s\,c_0\end{pmatrix}, \tag{A9}$$

with

$$p_\pm=\frac{d_0\cdot\exp[-R_\pm^2/(4\tau)]}{16\mu_0\sigma\sqrt{\pi^3\tau^5}}\,,\quad \overline{p}=\frac{d_0\cdot\exp[-\overline{R}^2/(4\tau)]}{8\mu_0\sigma\pi^2\tau^2\sqrt{r\,r_0}}\,. \tag{A10}$$

Due to (A5), the diffraction tensors $\dot{\mathscr{H}}^e$ and $\dot{\mathscr{E}}$, defined in (A6) and (3.44), are related by

$$\dot{\mathscr{H}}^e(\mathbf{r}|\,\mathbf{r}_0;\,t)=-\frac{d_0}{\mu_0 m_0}\cdot\dot{\mathscr{E}}^{\mathrm{T}}(\mathbf{r}_0|\,\mathbf{r};\,t)\,. \tag{A11}$$

No simple expression is known for the transient electric field of an electric dipole. However, its time derivative is easily obtained from the time derivative of the magnetic field via $\dot{\mathbf{E}}^e=(1/\sigma)\nabla\times\dot{\mathbf{H}}^e$. Let

$$\dot{\mathbf{E}}^e(\mathbf{r}|\,\mathbf{r}_0;\,t)=\dot{\mathscr{E}}^e(\mathbf{r}|\,\mathbf{r}_0;\,t)\,\tilde{\mathbf{d}}\,, \tag{A12}$$

with

$$\dot{\mathscr{E}}^e=w_-\dot{\mathscr{E}}^e_-+w_+\dot{\mathscr{E}}^e_++\dot{\mathscr{F}}^e\,. \tag{A13}$$

Then the diffraction tensors are given by

$$\dot{\mathscr{E}}^e_\pm=q_\pm\cdot\begin{pmatrix}\xi^2+\Delta_\pm & \xi\eta & \mp\xi\zeta_\pm\\ \xi\eta & \eta^2+\Delta_\pm & \mp\eta\zeta_\pm\\ \xi\zeta_\pm & \eta\zeta_\pm & \mp(\zeta_\pm^2+\Delta_\pm)\end{pmatrix}, \tag{A14}$$

$$\dot{\mathscr{F}}^e=\overline{q}\cdot\begin{pmatrix}2rr_0\,s\,s_0 & -\xi r\,s\,s_0 & -\xi r\,s\,c_0\\ \xi r_0\,s\,s_0 & (\Delta+2rr_0)\,s\,s_0 & (\Delta+r_0^2+rr_0)\,s\,c_0\\ \xi r_0\,c\,s_0 & (\Delta+r^2+rr_0)\,c\,s_0 & [\Delta+(r+r_0)^2]\,c\,c_0\end{pmatrix}, \tag{A15}$$

with

$$\Delta_\pm:=4\tau-R_\pm^2\,,\quad \Delta:=3\tau-r^2\cos\varphi-r_0^2\cos\varphi_0-\overline{R}^2\,, \tag{A16}$$

$$q_\pm:=\pm\frac{d_0\cdot\exp[-R_\pm^2/(4\tau)]}{32\mu_0\sigma^2\sqrt{\pi^3\tau^7}}\,,\quad \overline{q}:=-\frac{d_0\cdot\exp[-\overline{R}^2/(4\tau)]}{16\mu_0\sigma^2\pi^2\tau^3\sqrt{r\,r_0}}\,. \tag{A17}$$

$\dot{\mathscr{F}}^e$ decays as t^{-2}. Therefore, $\mathscr{E}^e$ shows an extremely slow $1/t$ decay, whereas $\mathscr{E}^m := \mathscr{E}$ decays as t^{-2} (eqs 3.44–3.48). Reciprocity is again guaranteed by the symmetry

$$\dot{\mathscr{E}}^e(\mathbf{r}|\mathbf{r}_0; t) = [\dot{\mathscr{E}}^e(\mathbf{r}_0|\mathbf{r}; t)]^{\mathrm{T}} . \tag{A18}$$

Although $\dot{\mathbf{E}}^e$ has a similar structure to $\dot{\mathbf{H}}^m$ given in (3.25)–(3.30), the different boundary conditions introduce substantial changes.

APPENDIX B: HORIZONTAL PERFECTLY CONDUCTING HALF-PLANE IN A LAYERED HOST

A perfectly conducting half-plane at $z=0$, $y \geq 0$ embedded in a layered host with conductivity distribution $\sigma(z)$, $-\infty < z < +\infty$ is considered. The treatment is given in the frequency domain and subsequently transformed into the time domain. For $z \neq 0$ and outside the sources the electromagnetic field can be presented by a toroidal scalar $\tilde{T}$ and a poloidal scalar $\tilde{P}$ as

$$\tilde{\mathbf{H}} = \nabla \times \nabla \times (\hat{\mathbf{z}} \tilde{T}) + \sigma \nabla \times (\hat{\mathbf{z}} \tilde{P}), \tag{B1}$$

$$\tilde{\mathbf{E}} = -i\omega\mu_0 \nabla \times (\hat{\mathbf{z}} \tilde{T}) + (1/\sigma) \nabla \times \nabla \times (\hat{\mathbf{z}} \sigma \tilde{P}) \tag{B2}$$

with

$$\nabla^2 \tilde{T} = k^2 \tilde{T}, \quad \nabla \cdot \{(1/\sigma) \nabla (\sigma \tilde{P})\} = k^2 \tilde{P} \quad \text{and} \quad k^2 = i\omega\mu_0\sigma . \tag{B3}$$

(In an insulator we assign a small constant value to σ, such that in B2 the conductivity drops out.) Noting that $\sigma \nabla \times (\hat{\mathbf{z}} \Psi) = \nabla \times (\hat{\mathbf{z}} \sigma \Psi)$, it is seen that the current density $\tilde{\mathbf{J}} = \sigma \tilde{\mathbf{E}}$ and the magnetic field $\tilde{\mathbf{H}}$ are solenoidal. For illustration we confine our attention to the simplest case, namely the vertical magnetic field of a vertical magnetic dipole, where the source can be described by purely toroidal current flow and where also the scattered field component depends only on the anomalous toroidal currents.

As in Section 5, all field components are separated into a normal and an anomalous part, e.g. $\tilde{T} = \tilde{T}_n + \tilde{T}_a$, where the latter is generated by the half-plane. In the sequel the field components are considered in the Fourier domain of the horizontal wavenumber $\boldsymbol{\kappa} = u\hat{\mathbf{x}} + v\hat{\mathbf{y}}$, e.g.

$$\tilde{T}(\mathbf{r}) = \frac{1}{4\pi^2} \int\int_{-\infty}^{+\infty} \hat{T}(z, \boldsymbol{\kappa}) \, e^{i\boldsymbol{\kappa}\cdot\mathbf{r}} \, d^2\boldsymbol{\kappa}, \tag{B4}$$

where $\tilde{T}$ and $\hat{T}$ may actually present the total, normal or anomalous field. Let

$$\kappa^2 := \boldsymbol{\kappa}^2 = u^2 + v^2, \quad \varkappa^2(z) := \kappa^2 + k^2(z) . \tag{B5}$$

Then the transformed toroidal and poloidal scalars $\hat{T}$ and $\hat{P}$ outside the sources satisfy

$$\hat{T}'' = \varkappa^2 \hat{T}, \qquad \{(1/\sigma)(\sigma\hat{P})'\}' = \varkappa^2 \hat{P} . \tag{B6}$$

The normal field has its source at the dipole level $z=z_0$ and the anomalous field at the half-plane level $z=0$. Let $z=z_s$ be the generic source level. The toroidal Green's function $f_T(z|z_s, \kappa)$ satisfying

$$f_T'' = \varkappa^2 f_T - \delta(z - z_s) \tag{B7}$$

is required in the following. Let $f_\pm(z)$ be two non-zero solutions of the homogeneous version of (B7), vanishing for $z \to \pm\infty$ respectively. Then

$$f_T(z|z_s) = \frac{1}{B_T^+ + B_T^-} \begin{cases} f_-(z)/f_-(z_s), & z \leq z_s \\ f_+(z)/f_+(z_s), & z \geq z_s \end{cases}$$

$$\text{with} \quad B_T^\pm := \mp \left. \frac{\partial_z f_\pm}{f_\pm} \right|_{z=z_s \pm 0} . \tag{B8}$$

As a Green's function, f_T satisfies the reciprocity relation

$$f_T(z|z_s) = f_T(z_s|z) . \tag{B9}$$

A vertical magnetic dipole with moment $\tilde{m}$ at $\mathbf{r}_0$ is in terms of f_T represented as

$$\hat{T}_n(z, \boldsymbol{\kappa}) = \tilde{m} f_T(z|z_0, \kappa) \, e^{-i\boldsymbol{\kappa}\cdot\mathbf{r}_0}, \tag{B10}$$

whereas $\hat{P}_n \equiv 0$.

The perfectly conducting half-plane at $z=0$, $y \geq 0$ is taken into account by requiring that at $z=0$ the (total) tangential electric field vanishes at the half-plane and that no sheet currents are flowing in $y<0$ (whereas they exist in $y>0$). Therefore,

$$\hat{\mathbf{z}} \times \tilde{\mathbf{E}} = -i\omega\mu_0 \nabla_h \tilde{T} + \hat{\mathbf{z}} \times \nabla \{(1/\sigma)\partial_z(\sigma \tilde{P}_a)\} = 0 \quad \text{for} \quad y > 0 \tag{B11}$$

and

$$\hat{\mathbf{z}} \times \tilde{\mathbf{H}}_a \big|_{-0}^{+0} = \{\hat{\mathbf{z}} \times \nabla \partial_z \tilde{T}_a + \sigma \nabla_h \tilde{P}_a\} \big|_{-0}^{+0} = 0 \quad \text{for} \quad y < 0, \tag{B12}$$

where ∇_h is the projection of ∇ into the (x, y)-plane. The insertion of these conditions into the Fourier representations of $\tilde{T}_a$ and $\tilde{P}_a$ then leads to four scalar equations, which for given $\hat{T}_n(v) := \hat{T}_n(0, \boldsymbol{\kappa})$ form a system of coupled dual integral equations for the unknowns $\hat{T}_a(v) := \hat{T}_a(0, \boldsymbol{\kappa})$ and $\hat{Q}_a(v) := (1/k^2)\partial_z\{\sigma \hat{P}_a(z, \boldsymbol{\kappa})\}|_{z=0}$:

$$\int_{-\infty}^{+\infty} [u\hat{T}_a(v) + v\hat{Q}_a(v)] \, e^{ivy} \, dv = -\int_{-\infty}^{+\infty} u\hat{T}_n(v) \, e^{ivy} \, dv, \quad y > 0, \tag{B13}$$

$$\int_{-\infty}^{+\infty} [v\hat{T}_a(v) - u\hat{Q}_a(v)] \, e^{ivy} \, dv = -\int_{-\infty}^{+\infty} v\hat{T}_n(v) \, e^{ivy} \, dv, \quad y > 0, \tag{B14}$$

$$\int_{-\infty}^{+\infty} [uG_T(v)\hat{T}_a(v) + vG_P(v)\hat{Q}_a(v)] \, e^{ivy} \, dv = 0, \quad y < 0, \tag{B15}$$

$$\int_{-\infty}^{+\infty} [vG_T(v)\hat{T}_a(v) - uG_P(v)\hat{Q}_a(v)] \, e^{ivy} \, dv = 0, \quad y < 0, \tag{B16}$$

where

$$G_T := B_T^+ + B_T^- \quad \text{and} \quad G_P := k_+^2 / B_P^+ + k_-^2 / B_P^- \tag{B17}$$

with $k_\pm^2 := k^2(z = \pm 0)$ and

$$B_T^\pm := \mp \partial_z \hat{T}_a / \hat{T}_a|_{z=\pm 0}, \quad B_P^\pm := \mp \partial_z(\sigma\hat{P}_a)/(\sigma\hat{P}_a)|_{z=\pm 0} . \tag{B18}$$

By linear combination and differentiation (equivalent to the application of the operators $\nabla_h \cdot$ and $\hat{\mathbf{z}} \cdot \nabla \times$ to B11 and B12, $y \neq 0$) these equations are easily decoupled. Then the resulting

dual integral equations for $\hat{T}_a$ and $\hat{Q}_a$ are

$$\int_{-\infty}^{+\infty} \kappa^2 \hat{T}_a(v)\, e^{ivy}\, dv = -\int_{-\infty}^{+\infty} \kappa^2 \hat{T}_n(v)\, e^{ivy}\, dv, \quad y>0, \tag{B19}$$

$$\int_{-\infty}^{+\infty} \kappa^2 G_T(v)\hat{T}_a(v)\, e^{ivy}\, dv = 0, \quad y<0 \tag{B20}$$

and

$$\int_{-\infty}^{+\infty} \kappa^2 \hat{Q}_a(v)\, e^{ivy}\, dv = 0, \quad y>0, \tag{B21}$$

$$\int_{-\infty}^{+\infty} \kappa^2 G_P(v)\hat{Q}_a(v)\, e^{ivy}\, dv = 0, \quad y<0. \tag{B22}$$

For a given conductivity profile $\sigma(z)$ the solutions of (B6), vanishing in both directions of the source level $z=0$, are readily calculated. In particular, if $\sigma(z)$ consists of uniform layers, $\hat{T}_a$, $\partial_z\hat{T}_a$, $\sigma\hat{P}_a$ and $\partial_z\hat{P}_a$ are continuous at layer boundaries. Therefore, the transfer functions $B^{\pm}_{P,T}$ and the system functions $G_{P,T}$ can be assumed to be known. Then the formal solution of the dual integral equations is obtained by the Wiener–Hopf technique, preferably using the version of Clemmow (1951). The key step is the splitting of the system functions into the ratio of two functions, which are holomorphic and free of zeroes in the complex lower v half-plane (K_- and L_-) and upper v half-plane (K_+ and L_+),

$$G_T(v) = K_-(v)/K_+(v), \quad G_P(v) = L_-(v)/L_+(v). \tag{B23}$$

These split functions are given by

$$\log K_{\pm}(v) = -\frac{1}{2\pi i}\int_{-\infty}^{+\infty} \log G_T(w)\, \frac{dw}{w-v\mp i\epsilon} \tag{B24}$$

(and similarly for G_P), where the small positive quantity ϵ is introduced only to warrant that—for real v and w—the contour in the w-plane is indented below the point v for $K_+(v)$ and above the point v for $K_-(v)$. Since the system functions depend via κ only on v^2, we have the symmetries

$$K_+(v)K_-(-v)=1, \quad L_+(v)L_-(-v)=1. \tag{B25}$$

valid for all complex v. Then the solutions of the dual integral equations are

$$\hat{T}_a(v) = \frac{K_+(v)}{2\pi i\kappa^2}\left[A + \int_{-\infty}^{+\infty} \frac{\lambda^2 \hat{T}_n(w)\, dw}{K_+(w)(w-v+i\epsilon)}\right], \tag{B26}$$

$$\hat{Q}_a(v) = \frac{L_+(v)}{2\pi i\kappa^2}\cdot B, \tag{B27}$$

where $\lambda^2 := u^2+w^2$ and A and B are arbitrary constants (independent of v, but dependent on u). Inserting these functions into (B19)–(B22) and closing the contours for $y>0$ in the upper v half-plane and for $y<0$ in the lower v half-plane by non-contributing great semi-circles, it is found that (B19)–(B22) are satisfied. The coupling constants A and B are now determined from the fact that the original four equations (B13)–(B16), from which (B19)–(B22) are derived, require for a special choice of A and B in order to be satisfied. Insertion of (B26) and (B27) into (B13) or (B14) and (B15) or (B16) yields a system of linear equations for A and B with the solution

$$A = \int_{-\infty}^{+\infty} \frac{\hat{T}_n(w)}{K_+(w)}\left[-w+i|u|\,\frac{L_+^2(i|u|)-K_+^2(i|u|)}{L_+^2(i|u|)+K_+^2(i|u|)}\right] dw, \tag{B28}$$

$$B = -\frac{2uL_+(i|u|)K_+(i|u|)}{L_+^2(i|u|)+K_+^2(i|u|)}\cdot\int_{-\infty}^{+\infty} \frac{\hat{T}_n(w)}{K_+(w)}\, dw. \tag{B29}$$

Since attention will be confined to $\tilde{H}_{zza}$, only $\hat{T}_a$ is required. Now,

$$\tilde{H}_{zza}(\mathbf{r}) = -\nabla_h^2\tilde{T}_a(\mathbf{r}) = \frac{1}{4\pi^2}\int\!\!\int_{-\infty}^{+\infty} \kappa^2\hat{T}_a(z,\boldsymbol{\kappa})\, e^{i\boldsymbol{\kappa}\cdot\mathbf{r}}\, d^2\boldsymbol{\kappa} \tag{B30}$$

and

$$\frac{\hat{T}_a(z,\boldsymbol{\kappa})}{\hat{T}_a(0,\boldsymbol{\kappa})} = \frac{f_T(z|0,\kappa)}{f_T(0|0,\kappa)} = f_T(z|0,\kappa)G_T(v) = f_T(z|0,\kappa)\,\frac{K_-(v)}{K_+(v)}. \tag{B31}$$

Therefore, assembling all intermediate results,

$$\tilde{H}_{zza}(\mathbf{r}|\mathbf{r}_0) = \int\!\!\int\!\!\int_{-\infty}^{+\infty} a(u,v,w)\cdot M(u,v,\mathbf{r})M(-u,-w,\mathbf{r}_0)\, du\, dv\, dw, \tag{B32}$$

with

$$M(u,v,\mathbf{r}) := f_T(z|0,\kappa)\, e^{i\boldsymbol{\kappa}\cdot\mathbf{r}}\cdot K_-(v) \tag{B33}$$

and

$$a(u,v,w) := \frac{\tilde{m}}{8\pi^3 i}\left[\frac{u^2+vw}{w-v+i\epsilon} + i|u|\,\frac{L_+^2(i|u|)-K_+^2(i|u|)}{L_+^2(i|u|)+K_+^2(i|u|)}\right]. \tag{B34}$$

Because $a(u,v,w)=a(-u,-w,-v)$, the change of variables $u\to -u$, $v\to -w$ and $w\to -v$ confirms the reciprocity $\tilde{H}_{zza}(\mathbf{r}|\mathbf{r}_0)=\tilde{H}_{zza}(\mathbf{r}_0|\mathbf{r})$.

Finally, let us consider two simple examples.

(1) *Uniform full space* $\sigma(z)=\sigma=$const.
Let $k^2 := i\omega\mu_0\sigma$, $\alpha^2 := \kappa^2+k^2$. Then

$$B_T^{\pm} = B_P^{\pm} = \alpha, \quad f_T(z|0,\kappa) = \frac{e^{-\alpha|z|}}{2\alpha} \tag{B35}$$

and

$$G_T(v) = 2\alpha, \quad K_-(v) = \sqrt{2(\gamma+iv)}, \quad K_+(v) = 1/\sqrt{2(\gamma-iv)}, \quad \gamma^2 := u^2+k^2, \tag{B36}$$

$$G_P(v) = 2k^2/\alpha, \quad L_-(v) = \sqrt{2k^2/(\gamma+iv)}, \quad L_+(v) = \sqrt{(\gamma-iv)/(2k^2)}. \tag{B37}$$

In this simple case, the triple integral (B32) can be performed in closed form (using transformations similar to those of Weidelt 1983, Appendix B) and after adding the normal field, (2.35) is retained.

(2) *Uniform half-space* $\sigma(z)=0$ for $z<-D$ and $\sigma(z)=\sigma$ for $z>-D$.
Let $k^2 := i\omega\mu_0\sigma$, $\alpha^2 := \kappa^2+k^2$. Then

$$B_T^{+} = B_P^{+} = \alpha, \quad B_T^{-} = \alpha\,\frac{\kappa+\alpha\tanh(\alpha D)}{\alpha+\kappa\tanh(\alpha D)}, \quad B_P^{-} = \alpha\coth(\alpha D). \tag{B38}$$

With transmitter and receiver at the air–earth interface, $z=z_0=-D$, we have

$$f_T(-D|0,\kappa)=\frac{\mathrm{e}^{-\alpha D}}{\kappa+\alpha}. \tag{B39}$$

The split functions cannot be given in closed form. However, the numerical evaluation is greatly simplified by subtracting the full-space response. This model has been used to compute the half-space response in Fig. 8.

If the v- and w-integrations are performed on the real axis, the interpretation of a typical Cauchy integral is

$$\int_{-\infty}^{+\infty}\frac{f(w)\,dw}{w-v\mp i\epsilon}=\pm i\pi f(v)+\mathrm{PV}\int_{-\infty}^{+\infty}\frac{f(w)\,dw}{w-v}, \tag{B40}$$

where PV denotes the Cauchy principal value.

With $\tilde{m}=-m_0/(i\omega)$, the transients are obtained from

$$\dot{H}_{zza}(\mathbf{r}|\mathbf{r}_0;\,t)=\frac{1}{2\pi}\int_{-\infty}^{+\infty}i\omega\tilde{H}_{zza}(\mathbf{r}|\mathbf{r}_0;\,\omega)\,\mathrm{e}^{i\omega t}\,d\omega. \tag{B41}$$